The gas distribution in the central region of the Galaxy. V - (C-12)O in the direction of the Sagittarius source complex

Burton, W.B.; Liszt, H.S.

ASTRONOMY & ASTROPHYSICS
SUPPLEMENT SERIES

Astron. Astrophys. Suppl. Ser. **95**, 9-39 (1992)

The gas distribution in the central region of the Galaxy. V. ^{12}CO in the direction of the Sagittarius source complex

W.B. Burton[1] and H.S. Liszt[2,1]

[1] Sterrewacht Leiden, P.O. Box 9513, 2300 RA, Leiden, The Netherlands
[2] National Radio Astronomy Observatory, Edgemont Road, Charlotesville, Virginia, 22903-2475 U.S.A.

Received May 14; accepted November 14, 1991

Abstract. — We have observed ^{12}CO $j = 1 - 0$ emission on a 2′ grid over the Sgr A, B, and C source complex. The region exhibits intense emission from clouds associated with the continuum sources, but the dominant behavior arises in several larger-scale, coherent features (like the "rotating nuclear disk" and "expanding molecular ring") and much of the most interesting structure occurs perpendicular to the galactic plane. To explain the observations we invoke a model which modifies our earlier view of the inner-Galaxy material in detail but not in spirit: major kinematic features arise from smooth charges in large-scale velocity laws and galactic geometry, and are thus not discrete, spatially isolated entities. In the new model, the distribution of the gaseous material occurring in the inner few hundred pc is flat, aligned with the nominal galactic equator, and mostly rotating. At larger radii (roughly out to 1.5 kpc) the gas layer both warps and flares, resembling closely our earlier tilted disk models, and a strong (> 100 km/s) component of non-circular motion is pervasive.

Key words: galaxy: center — kinematics and dynamics — interstellar medium: molecules — radio lines: molecular: interstellar surveys.

1. Introduction.

In the earlier papers of this series – Burton & Liszt (1978; Paper I), Liszt & Burton (1978; Paper II), Liszt & Burton (1980; Paper III), Burton & Liszt (1983a; Paper IV) we discussed the gas distribution in the inner few kpc of the Galaxy based on surveys of HI and on limited sampling of the molecular (CO) gas. We showed that the kinematics and distributions of molecular and atomic gas are sensibly identical, and that the distribution and kinematics of the gas in the inner Galaxy can be understood in terms of a simple but pervasive deviation (tilt) away from the nominal galactic equator. We also showed that the velocity field in the inner Galaxy is not predominantly one of rotation, with occasional (albeit prominent) collimated radial motions, but one in which non-circular motions make substantial contributions everywhere sampled. The non-circular motions are most satisfyingly ascribed to circulation along elliptical orbits such as are expected in the presence of a bar (Paper III), or, perhaps more generally, a triaxial mass distribution (Vietri 1986; Binney *et al.* 1991; Gerhard 1991). Bally *et al.* (1988) attributed some large cloud complexes in the galactic center, notably Sgr B, to the dust lanes associated with a central bar. Stark *et al.* (1991) suggested that these complexes must inevitably begin to fall to the center of the Galaxy, undergoing either a starburst of a catastrophic expulsive event.

The tilted distribution is known to characterize much of the material in the galactic bulge region. This tilt is shared by the atomic gas as well as the molecular gas (see, in addition to our own work cited above, also Kerr 1967; Cohen 1975; Cohen & Davies 1976; Sinha 1979 and Sanders *et al.* 1984); for these spectral-line tracers, it is evident that the tilted plane is the fundamental plane of symmetry both of the kinematics and of the geometry. The kinematic information represents an important advantage of the spectral tracers over continuum ones, but we note that an advantage of the infrared continuum tracers over the gas tracers is that a substantial component of the total mass is observed directly in the infrared: the tilted geometry in the bulge region is representative of the population of old stars as revealed by the 2.4-micron radiation observed by Matsumoto *et al.* (1982) and analyzed by Blitz & Spergel (1991), and of AGB stars in the IRAS Point Source Catalog (1985) studied by Weinberg (1991).

The earlier work notwithstanding, however, one has only to look at a radio continuum survey (for example, Fig. 1 of Downes *et al.* 1978, or Fig. 8.1 of Liszt, 1988) to realize that at least some portions of the inner-Galaxy gas distribution are both thin and closely aligned with

the nominal galactic plane. The radio continuum sources Sgr A, B, C, and D lie in a narrow band centered approximately at the latitude of Sgr A*, the compact radio source in Sgr A (i.e., at $b = -0.^\circ05$).

Because each of these HII-region complexes is associated with molecular material, as typically is the case in the Milky Way, it follows that there is a substantial mass of neutral gas at radii < 100-200 pc whose distribution also follows the galactic plane and is not described by the geometry of our earlier models. The strongest molecular emission seen in Sagittarius (Liszt *et al.* 1977) is the molecular analog of the rotating nuclear disk of early HI studies (see Oort 1977), although, as will become evident below and as was stressed in Papers I and II, simple rotation alone is not an adequate characterization of any inner-Galaxy gas.

To address the innermost material, the large-scale description of our earlier work is here supplemented by discussion of finer-scale CO observations taken in the direction of the Sagittarius source complex at $-0.^\circ6 < l < 0.^\circ8$, $-0.^\circ2 < b < 0.^\circ4$. The bounds of the survey grid are shown in relationship to the radio continuum morphology in Figure 1. The focus of this work, however, is not on detailed associations between ionized and neutral material (see Liszt *et al.* 1985), but on kinematic trends which cover the region as a whole and unavoidably involve material outside the Sgr A complex. As turned out to be the case earlier, the most interesting behavior seen even in this region occurs well away from the galactic equator.

Technical aspects of our observations are discussed in Section 2. Section 3 is a detailed taxonomy of the various and complicated kinematics of the molecular analog of the HI rotating nuclear disk, with some necessary diversions to account for other material. Section 4 describes a kinematic model, along the lines of those in Papers I-III, which serves as a crude vehicle for joining the material seen at larger and smaller radii within the inner galactic regions. We note that the radial extent of the gas discussed in this paper corresponds roughly to the extent of the galactic bulge. The kinematic and size scales used in this paper correspond to the galactic-constant values of $R_0 = 10.0$ kpc and $\Theta_0 = 250$ km/s; observed radial velocities are expressed with respect to the Local Standard of Rest. At the distance of Sgr A, 1° corresponds to 175 pc.

2. Observations.

The ^{12}CO observations were taken with the 36-foot telescope of the National Radio Astronomy Observatory on Kitt Peak, used in conjunction with Schottky-diode mixers. Some 750 spectra were gathered during observing runs carried out between September, 1978, and May, 1982. All observations were taken on a somewhat irregularly-bounded grid of 2-arcminute beam spacings extending between Sgr C and Sgr B, at $-0.^\circ5 < l < 0.^\circ8$, $-0.^\circ2 < b < 0.^\circ4$ (see Fig. 1). The data were taken with 256 filter channels, each 1 MHz (2.6 km/s) wide, usually in each of two polarizations. The integration times were varied so as to keep the noise approximately uniform and below 0.3 K (rms).

In presenting the observations below, the coordinates are described relative to the position of the compact radio source Sgr A*, at $l = -0.^\circ05$, $b = -0.^\circ05$. The units of intensity are brightness temperature above the cosmic background, corrected for all the usual losses and scaled up by a nominal main beam efficiency of 70 percent; we note that the less-than-perfect nature of the beam of the 36-foot telescope is of little consequence to the structures observed here, which are exceptionally intense and characterized by well-defined, coherent, localized behavior. The angular width of the main beam was approximately 70 arcseconds at the CO line, so that the survey region is relatively undersampled. This presents little problem for the discussion here, but finer sampling would be desirable for comparing the neutral gas distribution with that now mapped at high resolution in the radio continuum by many observers at the VLA.

3. Description and discussion of observed behavior.

The basic survey data are given in three complementary forms: in Figure 2, as a series of longitude-velocity diagrams at 4′ intervals in latitude; in Figure 3, as latitude-velocity diagrams at 4′ intervals in longitude; and in Figure 4 as a series of moment (integrated-intensity) maps. Each of these data forms is given a detailed discussion, but in general, we may distinguish three classes of behavior among the observed features or kinematic trends, with which we are concerned to varying degrees.

3.1. Material at $R > 2$ kpc.

First, we note the existence of gas lying outside the physical region of interest. This gas appears at low $|v|$ as the result of intervening clouds located in the Galaxy-at-large, probably well outside the bulge region. This gas is seen in both emission and absorption.

When the inner Galaxy is not sampled, as in the l, v diagrams at $\Delta b > 8'$, there is a clearly defined, narrow, zero-velocity feature. But when strong emission is present from the central regions, intervening material causes vertical stripes to appear (particularly at 0 and −17 km/s) in the position, velocity plane. The 3-kpc arm also appears in both ^{12}CO emission and absorption (see Bania 1980) in the l, v diagrams at $\Delta b = -8'$ and $-4'$ ($-60 < v < -40$ km/s), and is particularly easy to identify where projected against the Sgr C region (Liszt 1985) at $\Delta l = -30'$. The presence of several absorption lines in the range $-60 < v < 0$ km/s complicates the appearance of inner-Galaxy emission patterns at many negative longi-

tudes, but the absorbing gas itself can usually be readily discerned.

3.2. THE "EXPANDING MOLECULAR RING ".

Next, there is widespread emission from the "expanding molecular ring" features; this emission crosses zero longitude at −135 km/s and + 165 km/s. This behavior can be interpreted either in terms of real outflow (Scoville 1972; Liszt & Burton 1978) or in terms of a circulation pattern (Liszt & Burton 1980). In our earlier models, no discrete "ring" is required to explain the emission pattern: it is the consequence of projection effects over a wide range of galactocentric radii extending typically beyond several hundred pc; in a discrete ring model (Scoville 1972), the radius of the ring is about 150 pc.

The survey data amply demonstrate the distribution of the emission comprising the "expanding" molecular features. The positive-velocity material appears at generally higher latitudes (see the l, v maps at $|\Delta b| = 8'$ or almost any of the b, v diagrams) and both the positive- and negative-velocity emission patterns are seen at progressively more extreme latitudes as the longitude of observation increases. The latter behavior is especially apparent in the integrated-intensity maps at $v < -120$ km/s and in the l, v diagrams at lower latitudes. In the l, v maps where both the positive and negative-velocity components are present, both are seen to have the same small velocity gradient in the sense of normal galactic rotation, and both clearly run the entire length of the diagram. The large linewidths of the emission and the great spatial extent (clearly to $\Delta l > 2°$ near the equator, as shown by Fig. 1 of Liszt & Burton 1978) argue for the kind of projective model we presented in the earlier papers of this series; the consistent behavior of the two portions of the feature (at positive and negative velocities) can be rather simply explained in terms of a single morphology. In fact, the longitude-latitude disposition and the latitude-velocity segregation of this emission are straightforward manifestations of the basic tilt geometry on which our models of Papers I-III are founded.

3.3. LONGITUDE-VELOCITY BEHAVIOR OF INNER-GALAXY MATERIAL; ASPECTS OF A ROTATION SIGNATURE.

Gas lying closer to the galactic center might be distinguished by the presence of a substantial velocity gradient $\Delta v/\Delta l > 0$ around $\Delta l = 0°$, and so should be especially apparent in l, v diagrams; inward-lying gas in which the predominant kinematics are those of rotation will exhibit an abrupt shift from negative to positive velocities in this region. Larger-scale l, v maps at $\Delta b = 0°$, as in Figure 1 of Paper II, show indeed that most of the very intense emission associated with the galactic center, and with the continuum sources Sgr A, B, and C, is characterized by such behavior. There are, however, two important exceptions to this behavior. The prominent zero-velocity crossing at $\Delta b = 0°$ occurs at substantially negative longitudes, and the "rotation" pattern is asymmetric in the sense that high positive velocities $v > 80$-100 km/s are not found. The velocity gradient mimicking rotation, present over the entire region $-120' < l < 20'$, -120 km/s $< v <$ 80-100 km/s, vanishes abruptly at higher longitudes. The general characteristics of this gas, which is the closest molecular analog of the HI rotating nuclear disk, are discussed by Liszt *et al.* (1977) and in Paper II.

The present data show that this pattern actually consists of two related parts which are offset in latitude by a few arcminutes, and in velocity by some 50 km/s, so that the longitude at which the zero-velocity crossing occurs is latitude-dependent. At $\Delta b = 0'$, the gas under discussion first appears strongly (for these data) in the vicinity of Sgr C near $\Delta l = -30'$, with peaks at −60 and −110 km/s. The emission pattern is clearly double between Sgr A and B ($0' < l < 50'$), where the velocity gradient has carried both parts through the complicated emission and absorption structure at low-to-moderate negative velocities. From comparison of the various l, v diagrams, one infers that the lower-velocity component occurs at somewhat higher latitude. Specifically, one may compare the map at $\Delta b = -4'$, where only the more positive-velocity part is apparent and the zero-velocity crossing occurs at $\Delta l = -10'$, with the map at $\Delta b = 8'$. In the latter, there appears to be a continuously traceable emission pattern extending from $\Delta l = -34'$, $v = -130$ km/s, to $\Delta l = +34'$, $v = 40 - 50$ km/s. There is no obvious intervening gas which could create such a doubled appearance through absorption, although the 3-kpc arm does appear in absorption at negative longitudes to split one or other of the pair individually (see the b, v maps at $l < -20'$ in Fig. 3).

As noted by Heiligman (1982), the presence of the two zero-velocity crossings (at positive and negative latitudes and longitudes) mitigates the asymmetry seen earlier for the stronger (lower-latitude, higher-velocity) part alone; taken together, the pair form a pattern which is roughly symmetric about zero velocity and longitude. But the absence of velocities $v > 100$ km/s at $\Delta l > 30'$ remains to be explained. The solution adopted by Gusten & Downes (1980), involving a rotating disk with much of the positive-longitude and positive-velocity parts absent, is unsatisfactory: what is "missing" is not the relevant emission, but a velocity gradient in that emission.

Comparison of the l, v diagrams indicates that the strong rotation signatures are narrowly confined in latitude. Of course, this is also a characteristic of the strong radio continuum emission (and sources) from the Sagittarius source complex and there is a direct connection between the two phenomena. The continuum sources Sgr A, B, C, etc., are each associated with molecular gas compo-

nents whose kinematics associate them with the "rotating" material. Around Sgr C ($\Delta l = -30'$) there are peaks in both the higher- and lower-velocity components. Near Sgr A, the 50 km/s molecular cloud which nests inside the radio continuum contours (Liszt *et al.* 1985) is readily associated with the higher-velocity component by the rotation signature. Sgr B, at $l = 40' - 50'$, is less prominent in CO but seemingly associated with the lower-velocity component.

3.4. Latitude-velocity behavior; the complement of the rotation signature.

We concluded the previous section by noting that both the pattern mimicking a strong rotational velocity gradient and the bulk of the radio continuum sources and strong CO emission are narrowly confined in latitude. If the inner-galaxy gas could be described solely as a thin disk in the plane of the larger Galaxy, and if the dominant gas motions occurred in this plane, latitude-velocity diagrams would add little to the immediately previous description. Of course, the −135 and +165 km/s features, which arise from material somewhat beyond 100-200 pc from the galactic center, cannot be characterized in such a manner, and the earlier papers (I-III) were devoted to exploiting the notion of a thin but tilted geometry for the large-scale behavior of galactic center material. In fact, the most interesting and novel behavior discovered in the course of the present work also occurs out of the nominal galactic plane, as we now discuss.

At large negative longitudes, the b, v diagrams show the slight latitude displacement of the two portions of the gas having a prominent rotation signature. For $\Delta l < -20'$, where the only contaminating foreground absorption against either part arises in the 3-kpc arm, the more-negative-velocity component is seen some 8′ to higher latitude. Although the two parts are not equally clearly visible in many of the b, v maps between $-16' < l < +12'$, they have both crossed zero velocity by $\Delta l = +16'$, where they are separated in velocity by approximately the same amount (40-50 km/s) as at $\Delta l < -20'$. As longitudes larger than +32′ (in the vicinity of Sgr B1 and B2) are approached, where little or no velocity gradient occurs in the higher-velocity portions, the lower-velocity component broadens in both velocity and latitude. The data suggest that Sgr B is associated with the lower-velocity of the two components of the rotation signature; its line profile shows pronounced alteration while that of its companion changes less.

Scanning the various b, v diagrams from lower to more-positive longitudes, an unexpected phenomenon is encountered for the first time at $\Delta l = -4'$; the higher-velocity part of the rotation signature gas stretches out to include higher latitudes and velocities. By $\Delta l = 12'$, this behavior covers almost 30′ in latitude and almost 100 km/s in velocity; at $\Delta l > 30'$, the peak velocity of the high-latitude extension is at +150 km/s, only slightly inward of the terminal velocity defined by the "expanding molecular ring" feature. At $\Delta l > 12'$, relatively little change occurs either in the maximum latitude extent of the feature or in its maximum velocity. Change in the latter can be ascribed to the effects of normal galactic rotation viewed at large distances from the galactic center.

Missing in our maps is a clear negative-latitude and negative-velocity counterpart, which would presumably extend out from the lower-velocity component of the gas exhibiting a rotation signature. We surmise that this is largely a consequence of the limited latitude coverage at the lower longitudes where such a feature would be most readily apparent. At positive longitudes, any counterpart would occur at low-to-moderate negative velocities where it could easily hide among the welter of structure induced by intervening material.

Thus, the positive velocities needed to complete the rotation signature at positive longitudes are present, but at some substantial remove from the galactic plane. However, it is unlikely that they result primarily from circular motion as is shown below in Section 4.

3.5. Maps of integrated intensity.

Figure 4 is a series of integrated intensity maps, spaced by, and summed over, 15 km/s. In general, such maps are not an adequate means of tracing the kinematic trends noted above *ab initio* but are useful after the fact and have some utility in identifying localized features ("clouds"). At the large negative velocities encountered in the first panel, the data show one of the large-scale tilts described in Papers I-IV. The material heads downward at more positive longitudes because the near side of the gas distribution is tipped down below the galactic plane (the circulation axis of the gas deviates from that of the Galaxy at large in such a way that it points – slightly – toward us), and because the major axis appears at negative latitude in the first quadrant of longitude. Velocities which cannot be produced by circular motion alone must appear below the apparent major axis.

In the range $-120 < v < -60$ km/s, there is little contamination from foereground or background gas and the survey extends sufficiently far into the fourth longitude quadrant that gas having large circular velocities is evident. Thus, around $v = -75$ km/s it is possible to discern separately the two components of the rotation signature; the higher-latitude, lower-velocity, portion appears in any given panel both above and at higher longitude than its companion. The stronger emission at velocities between −100 and −50 km/s around $\Delta l = -30'$ is associated with Sgr C (Liszt 1985). In the velocity interval $-30 < v < 0$ km/s, there is a noteworthy feature near zero latitude in the range $l = 0' - 10'$; Yusef-Zadeh (1987)

showed, using observations of Bally *et al.* (1987), that this little clump is associated with the thermal portions of the Sgr A radio continuum Arc.

At higher velocities, in the range $0 < v < 75$ km/s, the gas associated with both Sgr A and B becomes apparent; the 50 km/s cloud near Sgr A has an interesting morphological relationship to the Sgr A Arc which suggests a physical relationship between the two features (Liszt *et al.* 1985). Above 75 km/s, the high-latitude, higher-velocity extension noted above in Section 3.3 becomes apparent. Tracing the sequence of maps from lower to higher velocity, ones sees the feature first form at 75 km/s near $\Delta l = 5'$, extend in b at 90-105 km/s, and then arch over the galactic plane in the range 105-035 km/s. At higher velocities the effects of galactic rotation carry it along at nearly constant latitude; by 170 km/s the feature has moved beyond the spatial and velocity range of the observed material.

At the highest velocities included in the current observations, $v > 180$ km/s, the behavior of the emission pattern is complementary to that noted at the beginning of this section. Because of the large-scale tilts, the material – actually part of the "expanding molecular ring" feature, not the rotation signature gas – occurs substantially below zero latitude.

The concluding panel in Figure 4 is a map of intensity integrated over the entire range $|v| < 210$ km/s. Because the HII regions of the Sgr A complex are narrowly confined in latitude, and because they are associated with and so heat the surrounding molecular cloud complexes, the CO emission is similarly confined. Nonetheless it must be understood that this map is an amalgam of contributions from many aspects of the galactic center geometry. The latitude extent of the emission is not amenable to interpretation in terms of a thin disk lying in and aligned with the usual galactic disk.

4. A model based on a warped disk of gas which accounts for some of the trends identified in the CO observations.

4.1. INTRODUCTION.

We have tried to find a simple framework within which we may understand the range of trends observed in the galactic-core CO observations and listed above. Establishment of a plausible framework must necessarily precede a dynamical analysis. Most interpretive work on the inner-galaxy gas distribution and kinematics falls in either of two categories. The more widely used of these categories involves identification of discrete features such as spiral arms or rings. The second, and less widely used, category involves a more or less continuous distribution of gas, with the observed profile structure attributed to the vagaries of the viewing geometry.

The two approaches involve fundamentally different dynamical situations. The discrete-feature approach seems required when considering information from within an arcminute or so of the center. The time scales and linear scales involved are short enough that specific characteristics of a localized central engine may be reflected in the data. An example of this approach is given by the work on the galactic center minispiral. There are other observational phenomena whose association with the galactic core is revealed by their anomalous kinematics but which extend over lengths of up to a few kpc, and on these scales it has seemed reasonable in some cases to look not for discrete-feature ejection but, for example, for stable orbits which might arise as a response to a smooth gravitational potential. In our own work on the HI (Burton & Liszt 1978) and CO (Liszt & Burton 1978) in the inner few kpc of the Galaxy, we showed that neither kinematic nor density perturbations are necessarily implied by the existence of anomalous spectral features. These features may be consequences of the transformation of emission from gas filling a nonplanar distribution with both radial and circular components of motion.

However, our earlier HI model referred to data measured on a scale of tens of degrees, not tens of arcminutes as is the case for the present CO data. The difference in scale, together with the diversity of the trends enumerated for the present observations in the preceding sections caused our initial interpretive efforts to be directed toward a discrete-feature analyses. We were not successful in finding a plausible model (e.g., Burton & Liszt 1983b), and in particular there are several trends for which we can envision no discrete-feature explanation:

1) *Continuity in angle:* many of the principal features are continuously visible over the full angular extent of the grid, corresponding to more than 150 pc and possibly to kpc lengths, depending on projection. Outstanding examples are the "expanding molecular ring" at the edges of the emission distribution in Figure 2 at $\Delta b = -4'$, or the intermediate-velocity gas showing a stronger rotation signature at $| v | < 100$ km/s in the same diagram.

2) *Velocity gradients in the continuous structures:* changes of more than 100 km/s over angular scales of a few terms of arcminutes are clearly seen in the $b - v$ maps of Figure 3 at $\Delta l > 0'$.

3) *Large velocity widths:* the full extent of many of the observed features is quite large. The "expanding molecular ring" gas is about 100 km/s wide in Figure 2 at $\Delta b = -8'$ ($v < -100$ km/s). The strongly-emitting gas associated with Sgr B at $\Delta l = 44'$ in Figure 3 extends over some 125 km/s.

None of these characteristics pertains for emission from the galactic molecular-cloud ensemble. (That fact alone virtually ensures that the emission we are considering here comes from the galactic core). These characteristics are also incompatible with what is known of the physical

conditions in isolated molecular clouds. Individual components of the molecular ensemble have CO widths of order 5 km/s or less, and sizes measured in tens of parsecs. Velocity gradients in a cloud complex may involve 5 km/s; but in a isolated cloud the gradients are subtantially less. There are a few complexes of giant molecular clouds with embedded HII regions known, of the sort illustrated by W51, which do have widths of 10 to 20 km/s. But if such complexes dominated the present CO data they would certainly be evident in the VLA continuum data shown in Figure 1. In general, lack of continuum emission from the regions of the broad emission features seems to refute an explanation of the large widths as due to unusually high energetic levels, e.g., due to heating following star formation, in cloud complexes. It is in particular not easy to explain the gradient of 100 km/s, for which no other example is known.

Consequently we began to reconsider the possibility of finding a continuous-distribution model. Our earlier work on HI had shown (for the much larger scales) that gradients and continuity in position and in velocity as well as apparently high dispersions could result from the viewing geometry. Our earlier model involved a tilted but otherwise flat disk. No confinement to the plane is expected in that case for the integrated intermediate velocities; indeed, the intermediate velocity features were absent from our earlier model, and the predicted gradients are very different from those observed on the angular scales of the CO data. We therefore considered what changes were necessary in order to account for the trends enumerated above. We found a model which has some success in the inner-region CO data, but which at the same time is quite similar to our earlier model when viewed at larger radii.

4.2. Geometry of the warped, flaring disk model.

The geometry of the model is illustrated in Figure 5. Panel a) of that figure shows a cross-section of a disk with a flaring scale height. Within 200 pc of the center, the disk has a constant scale height (of 15 pc) with the central plane of the disk lying, uninclined, in the galactic equator $b = 0°$. At radii greater than 200 pc, the disk flares, to a scale height at 1.7 kpc of 150 pc. We introduced a warp to the outer, flaring, part of the disk, leaving the constant scale-height portion at $R < 200$ pc unperturbed.

The warp of the flaring part of the disk is analogous to the larger-scale warp observed in the outer parts of our own Galaxy as well as in M31. Thus the midplane of this gas layer makes an angle with respect to the galactic equator. This angle is constant along a given radius, so that the height of the flaring portion of the disk varies linearly along a radius. The warp angle varies sinusoidally with galactocentric azimuth (which is measured in the conventional way from 0° in the direction of the Sun increasing in the direction of galactic rotation). The line of nodes runs along the azimuth at which the warp angle crosses 0°.

Panel b) of Figure 5 shows a cross section on the plane of the sky (through azimuths 90° and 270°) for a maximum warp angle of 13°, and for the line of nodes rotated 45° from the Sun-center line. Shown in cross section are heights one scale height above and one below, the mean plane.

Panel c) shows the same section lines as in panel b), but with projected rings drawn corresponding to radii 900 pc, at the + and −1 scale-height levels. The outline of the observed grid is indicated. If one imagines a strip of observations made along the $l = 0°$ axis from the top of the grid to the bottom, one sees that – for the geometry pictured – lines of sight near the top of the grid intersect only portions of the flared disk above its midplane and beyond the galactic center; at the lower portions of the grid, the situation is reversed, with only the lower, nearer, portions of the disk intersected. In the center of the observed grid, near $b = 0°$, lines of sight traverse both upper and nearer, and lower and more distant, parts of the disk.

Panel d) of Figure 5 shows the situation for the full extent of the disk, with the flared portion continuing to 1.7 kpc. The ovals represent projections of rings, at 100 pc intervals, one scale height above and one below the mean gas layer. Note that the apparent tilt and inclination of the flared disk comes from the twist of the line of nodes as well as from the warp. The rings project as distorted ellipses because the projections are plotted in angular coordinates. Similarly the lines drawn at azimuths of 90° and 270° are not the major axes of the projected rings: this likewise can be attributed to the fact that the dimensions of the disk are not small with respect to the distance to the galactic center.

The crowding of the rings near the observed grid is particularly important to our interpretation. This crowding means that some lines of sight through a gas distribution of the sort incorporated in the model will traverse several kpc of gas. The crowding of the lines near the direction of the center makes it clear that closely adjacent lines of sight may sample grossly different sections of the disk, so that strong gradients might be expected. Note that these remarks would not pertain for a tilted plane-parallel disk of the sort used in our earlier work: the flare is necessary to cause different parts of the disk to occur along single lines of sight.

The geometry shown in Figure 5 is quite similar to that found for the flaring warp of our Galaxy (see e.g., Burton 1988) and of M31 (Brinks & Burton 1984). The formulation which we use when calculating synthetic profiles is a modification of that used by Brinks and Burton (1984) to model M31.

4.3. THE VELOCITY FIELD OF THE MODEL.

The appearance of the model gas distribution in the observed position-velocity space depends in a sensitive way on the kinematics. The observations are unambiguous in requiring both rotation and radial components. The signature of rotation is most clearly seen as the skewed shift of the l, v patterns from negative to positive velocities as the lines of sight shift from $l < 0°$ to $l > 0°$. The signature of radial motion is given in its most unambiguous form by the emission patterns at velocities different from zero at small l. On b, v maps near $l = 0°$, all non-zero velocities imply radial motions; that these motions are predominantly in the sense of expansion rather than contraction is proven by absorption information from HI, OH, H_2CO, and other lines.

The kinematics used in the model are plotted as a function of radius in Figure 6. These motions are intended to represent projections of the true velocity fields into pure-rotation and pure-expansion vectors. The actual shape of the particle orbits is a matter of dynamics, beyond the scope of this article. We note that it has been suggested, however, that the expansion vectors might come from motions in closed elliptical orbits (e.g., Peters 1975; Liszt & Burton 1980), or in orbits responding to a triaxial gravitational potential (see Binney *et al.* 1991; Gerhard 1991). Theoretical models of the gas dynamics in the inner kpc or so do not yet present a clear picture of the orientation of the velocity vectors, including those evidently required by strong $\Delta b/\Delta v$ gradients to lie not entirely in the galactic equator. Because the geometry which we are exploring in the core is so similar to that evidently pertaining in the warped gas layer of the outer parts of our Galaxy and of M31, one might speculate that the core structure reflects stable orbits within the potential of the bulge, just as the outer structure reflects stable orbits within the potential of the Galaxy as a whole. We do not address this point further here.

The motions in the model depend only on radius, not on height above the plane. Both the rotation and expansion components are represented, as simply as possible, by straight-line segments.

4.4. APPEARANCE OF THE MODEL IN SYNTHETIC LINE PROFILES.

We tested the model and adjusted its parameters by comparing synthetic line profiles with those observed. Such a procedure is practical because the transformation from spatial coordinates (as in Fig. 5) to the observed position-velocity coordinates is seldom easy to visualize. The transformation to line-of-sight velocities for a gas in circular orbits in a warped, flaring distribution is described by Brinks and Burton (1984) as adopted from the work of Burton and Liszt (1978). Addition of the expansion vector is straightforward.

The model contains about a dozen parameters, although the ones important in the present context are those describing the geometry (see Fig. 5) and the kinematics (see Fig. 6), because these are the parameters which dominate the manner in which the observed position-velocity space is populated. Description of the physical state of the gas is, of course, also necessary whenever calculating synthetic profiles; once chosen, however, we did not further adjust the temperature, density, or velocity dispersion. By holding these parameters constant, we stress that line-profile structure observed along long galactic lines of sight is commonly determined by the geometrical and kinematic situation pertaining along those lines of sight. Because all parameters were either held constant or vary slowly on the scale of the observed grid, it was not necessary to synthesize structure within the beam: a line beam suffices.

The temperature of the gas was held constant. The volume density in the mean plane was held constant throughout the flat inner disk of 200 pc radius. We assumed a Gaussian dependence on height above the midplane of the disk. The projected surface density remains constant throughout the entire structure. In order that this be the case in the flaring part of the disk the volume density in the mean plane decreases in a linear manner at $R > 200$ pc. The velocity dispersion of the gas was held constant throughout at a value of 7 km/s. This value was chosen to represent the combined effects of internal broadening of individual features, the apparent broadening caused by clumping of clouds into complexes, the fortuitous clustering from unrelated structures crowded in velocity but not in space, and the macroscopic cloud-cloud motions. The exact value of the dispersion parameter is not very important in the present context because it is substantially less than the width displayed by the modelled emission features. The dispersion parameter is reflected by the rather sharp kinematic cutoffs at the edges of both the observed and modelled features, not by the larger overall widths of these features. It is not implausible that the physical parameters of the gas might show some radial dependence on distance from the nucleus of the Galaxy, just as it is likely that there will be variations due to the localized environment. Any such dependences and variations are evidently not the dominant determinants of the principal position-velocity patterns considered here, although they may certainly be of importance in a different context; our investigation of consequences of kinematic and geometrical projections does not, for example, offer any insights into the thorny question of how CO intensity relates to molecular hydrogen mass. Suffice it to remark that we see no evidence in the data at hand for CO structures which would invalidate the usefulness of the simple parameterization for the present considerations of the shape and motions of the core gas.

The thickness of the gas layer varies in a normal distribution specified by its scale height. The CO observations provide quite robust restrictions on the vertical thickness. The integrated intermediate velocities shown in Figure 3 show that 15 pc is a reasonable height. We note that this is the height of the VLA continuum distribution shown in Figure 1. We note also, however, that this is a factor 3 or 4 less than that pertaining for the distribution of molecular clouds in the Galaxy at large.

The flaring to larger scale heights at larger R was indicated when searching for an optimized fit of the model to the observations. Some of the multiply-peaked structures can be accounted for as multiple passes of the line of sight through a constant-scale-height, warped disk: but warping into the line of sight is not sufficient by itself for other aspects of the observations. The lengths of path through the distribution must be quite long if the broad velocity widths of the sort observed are also to be displayed by synthesized profiles. Similarly, long lengths of path through the distribution are required for the continuous patterns with large gradients which are observed. The scale height reached at the edge of the warped disk, 150 pc at $R = 1.7$ kpc, is thicker than that of the CO gas layer in the molecular annulus at larger radii, but is of the same order as the scale height of the atomic gas throughout the inner Galaxy.

4.5. The rotation and expansion vectors.

The most direct information on the rotation field is given by the skewness of the emission patterns in l, v plots. We mention below two gradients in l, v space near $b = 0°$ which carry the most readily-interpreted data relevant to fixing the velocity components. The synthetic profiles respond to all adjustements to the kinematics; other aspects of the synthetic profiles were kept in mind as the kinematic characteristics of the model were optimized. For example, the strong positional and kinematic gradients in latitude, so clearly seen in the $b > 0°$, $l > 0°$, $v > 0$ km/s portions of the data cube, are one of the most striking aspects of the observations and an important challenge to any synthesis. Although our model does roughly reproduce this pattern, the influence of geometry and kinematics are intertwined in such a way that, in choosing parameters of the geometry and kinematics, attention is better paid to aspects of the observations where the dominant parameters can be identified.

We explored the parameter space, comparing synthesized l, v and b, v maps with the observed situation, and adjusting the geometric and kinematic parameters of the model in order to reproduce as much of the observed CO structure as possible. We know of no practical manner to optimize formally the fit of a multi-parameter model to a data cube of the sort available. As mentioned above, we did not further adjust the physical parameters, to which the simulated spectra were in any case not sensitive. Other than the parameters describing the shape of the gas layer, there are only two influential quantities, namely the rotation and expansion components, determining the kinematics.

The flat distribution of gas in the inner 200 pc at low and intermediate v exhibits a signature dominated by rotation in the l, v maps near $b = 0°$. This is especially evident in the ^{13}CO and CS data (Bally *et al.* 1987, 1988) for which the higher-density gas dominates. There is a zero-velocity cross-over near $l = 0°$, which could not be expected if substantial non-rotation motions were present in this region. This pattern is, however, broad in velocity. We find that a gradual increase from $R = 0$ to 200 pc of expansion velocity provides sufficient velocity gradients along the line of sight through the small flat disk to broaden the profiles in accordance with the observations.

The swath of emission which has been called the "expanding molecular ring", evident for example in l, v maps near $b = 0°$ crossing $l = 0°$ at $v = 160$ km/s unambiguously requires radial velocities. That these velocities are in the sense of expansion rather than contraction is revealed best by absorption in HI at the negative, but not the positive, velocities. The geometry of the model principally determines the radii at which the expansion velocities are intercepted. The model places the maximum expansion velocities in the range $0.8 < R < 1.0$ kpc. The expansion at smaller radii must be less. At radii larger than 1 kpc the expansion vector in the model decreases, although the relevant observational evidence is limited by the latitude extent of the observed grid. Within the context of the geometry of the model, the lines of sight within the observed grid traverse substantial lengths of path at $R > 1$ kpc. If the expansion term were to remain constant at its maximum value of 180 km/s, say, then there would be a pervasive spectral feature of very narrow velocity extent at the higher b. The observations show, instead, emission over a broad range of velocity; this is achieved in the simulation by having the amplitude of the expansion term drop at $R > 1.0$ kpc.

The rotation aspects of the kinematics are given principally by the slope of the emission pattern in l, v coordinates. The emission confined to the flat disk in the inner 200 pc shows the clearest rotation signature. The rotation curve which fits this region is indicated in Figure 6. The rotation plotted shows a much slower rise with distance from the center than that which would be derived assuming no expansion component in the motions (see e.g., Sanders & Lowinger 1972). The steepness of the rise is relevant to models of the galactic bulge; we note in passing that few external galaxies are known which have as steep a rise to an isolated peak as suggested in the no-expansion case for our own Galaxy.

The emission pattern associated with the expanding molecular feature shows a slope in l, v space which fixes

the rotation component in the mid- and outer-parts of the warped disk. The circular component of motion for gas lying about 1 kpc from the center is nearly perpendicular to lines of sight as close to the center as those observed. Consequently a rather large rotation component gives nevertheless a rather modest gradient. We find a satisfactory fit for a rotation component which rises to 250 km/s at the outer boundary of the disk. With this value of the rotation component, and with the expansion component going to zero at the edge of the disk, there is no discontinuity with the kinematics of the gas of the Galaxy at large at the boundary.

With only the geometrical and kinematic parameters dominating the model fitting, we found that the procedure quickly converged to a satisfactory simulation of the observed CO patterns. Our initial preconception was that the present CO work was done on a grid scale so much smaller than that of our earlier HI work that a very different model might be called for. Of the several thousand points observed in our earlier, inner-Galaxy HI survey on a half-degree grid, only three grid points are within the boundary of the CO data cube discussed here. Thus we were rather surprised when the model fitting procedure gave geometry, scale, and kinematics not very different from the Paper I HI model. Our interpretation involves CO data which, although restricted to relatively small angular extent, nevertheless involves material distributed along lengths of path of the kpc scale. Consequently, synthetic HI spectra calculated several degrees outside the observed CO grid but using the model geometry and kinematics of Figures 5 and 6 can reproduce as in Paper I most of the apparently anomalous HI features. We note also that the kinematics derived here for the CO distribution are consistent with those derived from a reanalysis of the the HI terminal velocities in which account is taken of the contamination by absorbing material.

5. Summary.

We presented observations of ^{12}CO $j = 1 - 0$ emission taken on a 2′ grid over the region of the source Sgr A, B, and C, ($-0.^{\circ}6 < l < 0.^{\circ}8$). These are displayed in the form of l, v and b, v position-*versus*-velocity diagrams and as a series of integrated-intensity (moment) maps, for the purpose of charting the gas distribution and kinematic behavior. Although there is strongly-emitting gas directly associated with each of the continuum sources, the data could only be fully understood in terms of structure accumulated along the very long paths (r kpc) traversed by the lines of sight through the galactic center gas. The major gas structures viewed in this region are *not individual clouds*, however broad-lined, but rather are kinematic features which exhibit a high degree of continuity in space and velocity and, often, velocity gradients which shift the lines over 100-200 km/s.

The most surprising aspect of the observations was found to be the extent to which structure occurs perpendicular to the galactic plane, in gas which is usually believed to be rather simply described as the molecular counterpart of the HI rotating nuclear disk. Even fairly close to $l = 0^{\circ}$ we found larger velocity shifts perpendicular to the galactic plane than along it. In a nominal sense these shifts relieve some of the strong kinematic asymmetries observed near $b = 0^{\circ}$, which previous observers had interpreted as the result of explosions and other esoteric phenomena in the galactic nucleus.

To accommodate the behavior seen in CO along and across the galactic plane, we presented a detailed kinematic and geometric model which modifies our earlier view of the inner-galaxy titled disk or bar (discussed in Papers I - III). In the new model, kinematic features are still created by the projection of large-scale galactic geometry and velocity fields but the innermost material is aligned with the galactic plane at large, and is mostly rotating. Only at somewhat larger radii, 200 – 300 pc, does the gas layer warp (i.e., become titled) and acquire a large and pervasive component of non-circular velocity. The model is largely able to account for the large linewidths as well as for the large velocity gradients observed to be characteristic of molecular-line emission from the region.

In view of the several analogies between the geometry of the warped gas layer in the core with that pertaining in the warped gas layer of the outer parts of our Galaxy and of M31, one might speculate that the core structure reflects stable orbits within the potential of the bulge, just as the outer structure reflects stable orbits within the potential of the Galaxy as a whole.

Acknowledgements.

The National Radio Astronomy Observatory is operated by Associated Universities, Inc., under contract with the National Science Foundation. This work was partially supported by a research grant (No. 008.82) from the North Atlantic Treaty Organization.

References

Bally J., Wilson R.W., Stark A.A., Henkel C. 1987, ApJS 65, 13

Bally J., Wilson R.W., Stark A.A., Henkel C. 1988, ApJ 324, 223

Bania T.M. 1980, ApJ 242, 95

Binney J.J., Gerhard O.E., Stark A.A., Bally J., Uchida K.I. 1991, MNRAS 252, 210

Blitz L., Spergel D.N. 1991, ApJ 379, 631

Brinks E., Burton W.B. 1984, A&A 141, 195

Burton W.B. 1988, in "Galactic and Extragalactic Radio Astronomy", Eds. G.L. Verschuur and K.I. Kellermann (Springer-Verlag) p. 295
Burton W.B., Liszt H.S. 1978, ApJ 225, 815 (Paper I)
Burton W.B., Liszt H.S. 1983a, A&AS 52, 63 (Paper IV)
Burton W.B., Liszt H.S. 1983b, in "Surveys of the Southern Galaxy", Eds. W.B. Burton and F.P. Israel (Reidel Pub. Co.) p. 149
Cohen R.J. 1975, MNRAS 171, 659
Cohen R.J., Davies R.D. 1976, MNRAS 175, 1
Downes D., Goss W.M., Schwarz U.J., Wouterloot J.G.A. 1978, A&AS 35, 1
Gerhard O.E. 1991, in proceedings workshop "Dynamics of Disk Galaxies", B. Sundelius, Ed., Goteborgs University, p. 111
Gusten R., Downes D. 1980, A&A 87, 6
Heiligman G. 1982, Ph.D. thesis, Princeton University
IRAS Point Source Catalog, 1985: Joint IRAS Working Group, Washington, D.C., U.S. Government Printing Office
Kerr F.J. 1967, in "Radio Astronomy and the Galactic System", H. van Woerden, Ed. (London: Academic Press) p. 239
Liszt H.S. 1985, ApJ 293, L65
Liszt H.S. 1988, in "Galactic and Extragalactic Radio Astronomy", Eds. G.L. Verschuur and K.I. Kellermann (Springer-Verlag) p. 359
Liszt H.S., Burton W.B. 1978, ApJ 226, 790 (Paper II)
Liszt H.S., Burton W.B. 1980, ApJ 236, 779 (Paper III)
Liszt H.S., Burton W.B., van der Hulst J.M. 1985, A&A 142, 245
Liszt H.S., Burton W.B., Sanders R.H., Scoville N.Z. 1977, ApJ 213, 38
Matsumoto T., Hayakawa S., Koizumi H., Murakami H., Uyama K., Yamagami T., Thomas J.A. in "The Galactic Center", Eds. G.R. Riegler and R.D. Blandford, AIP Conference Proc. 83, 48
Oort J.H. 1977, ARA&A 15, 295
Peters W.L. 1975, ApJ 196, 617
Sanders D.B., Solomon P.M., Scoville N.Z. 1984, ApJ 276, 182
Sanders R.H., Lowinger T. 1972, AJ 77, 292
Scoville N.Z. 1972, ApJ 175, L 127
Sinha R. 1979, in "The Large-Scale Characteristics of the Galaxy", W.B. Burton, Ed. (Dordrecht: Reidel Pub. Co.) p. 341
Stark A.A., Gerhard O.E., Binney J., Bally J. 1991, MNRAS 248, 14p
Vietri M. 1986, A&A 306, 48
Weinberg M.D. 1992, ApJ 384, 81
Yusef-Zadeh F. 1986, Ph.D. thesis, Colombia University

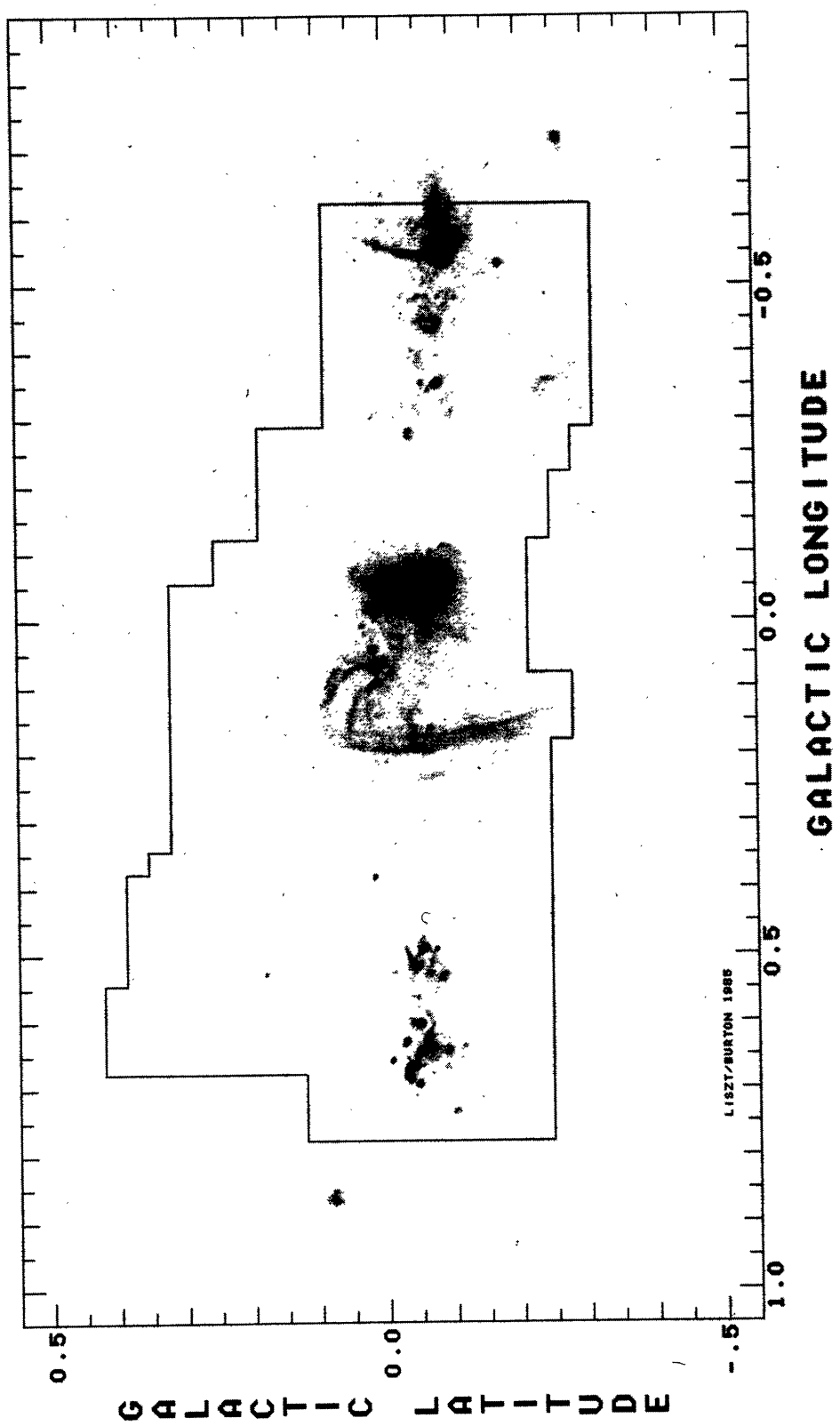

FIGURE 1. Boundaries of the present ^{12}CO survey shown superposed on a mosaic image of the 18-cm radio continuum taken at the VLA (Liszt 1988). From left to right, the bright sources are Sgr, B, A, and C, respectively. The apparent brightness of Sgr C has been adjusted upward for the sake of clarity.

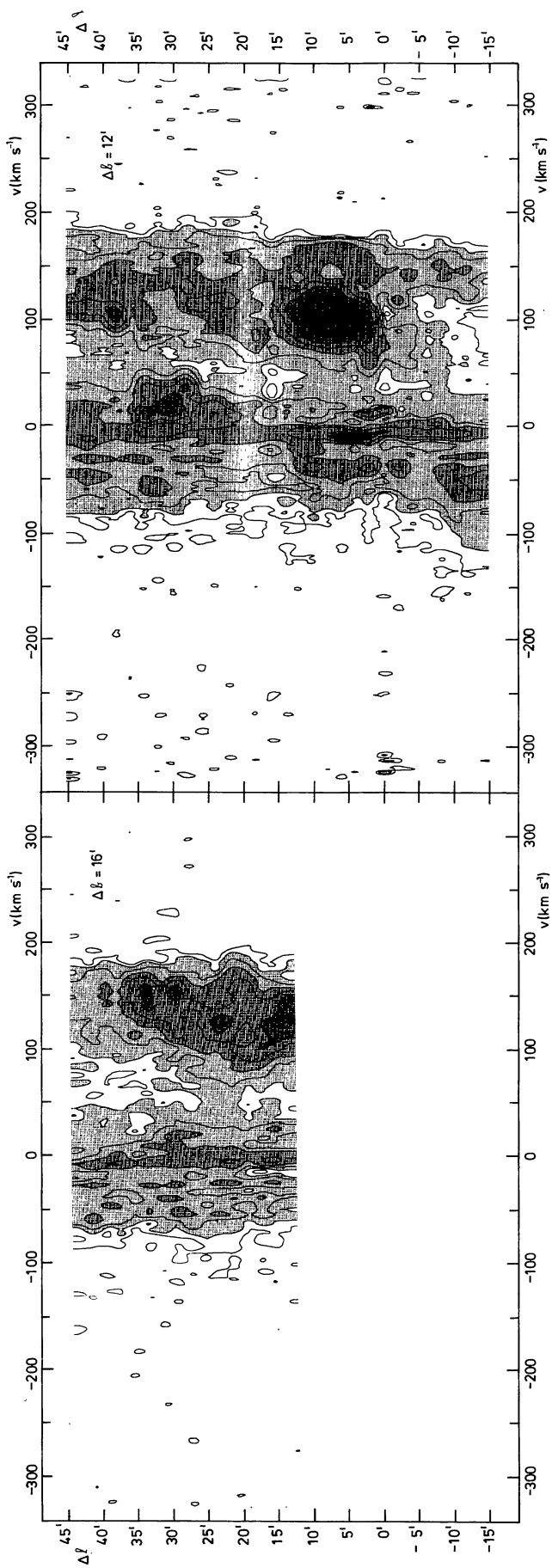

FIGURE 2a.

FIGURE 2. Longitude, velocity diagrams at 4′ intervals of galactic latitude; the longitude spacing of the data is 2′. Contour levels are drawn at 0.2, 0.4, 0.8, 1.5, 2.5, 4, 6, 8, 10, 13, 16, 20, 24, ... K. Coordinates in Figures 2, 3, and 4 are measured relative to the position of IRS 16/Sgr A* in Sgr A West.

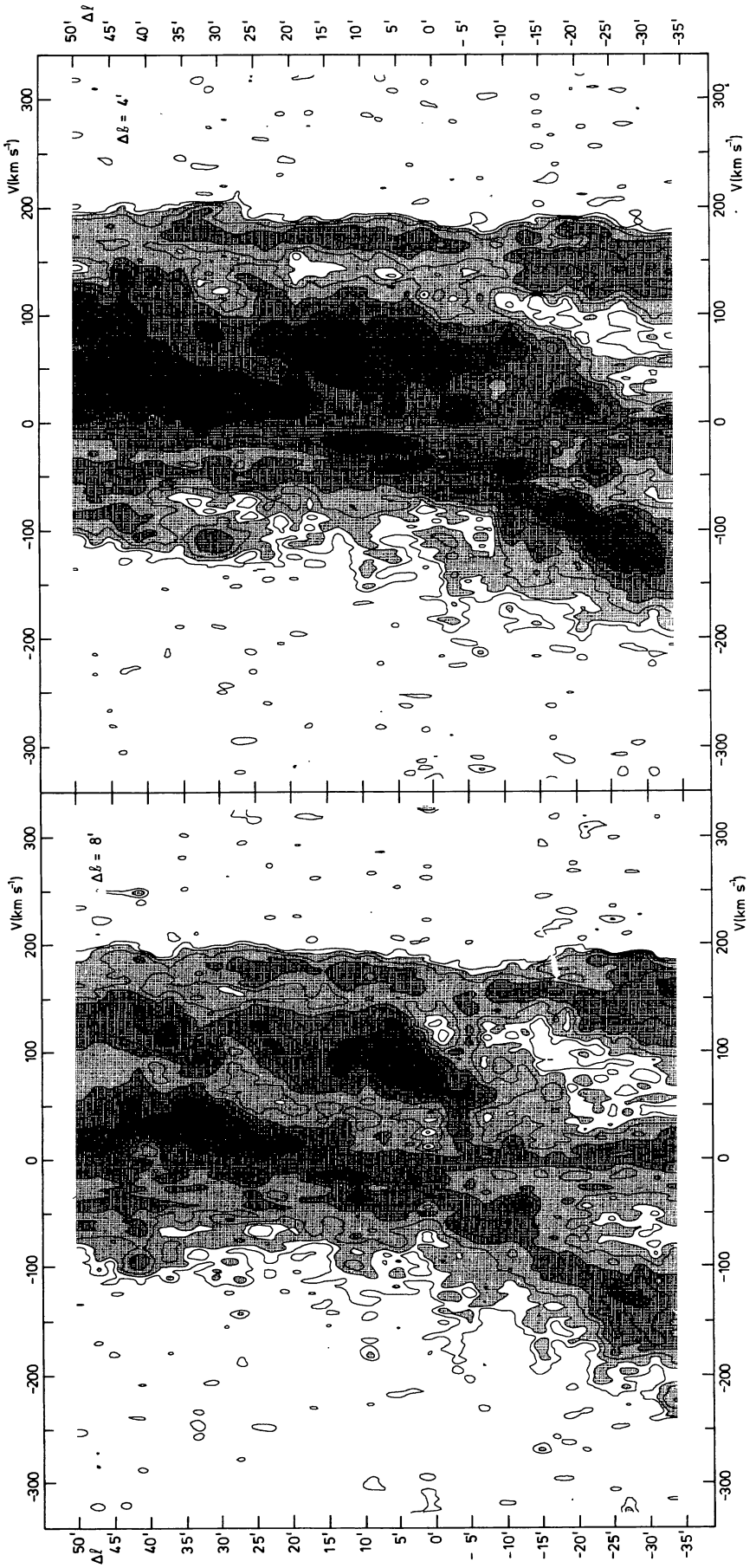

FIGURE 2b.

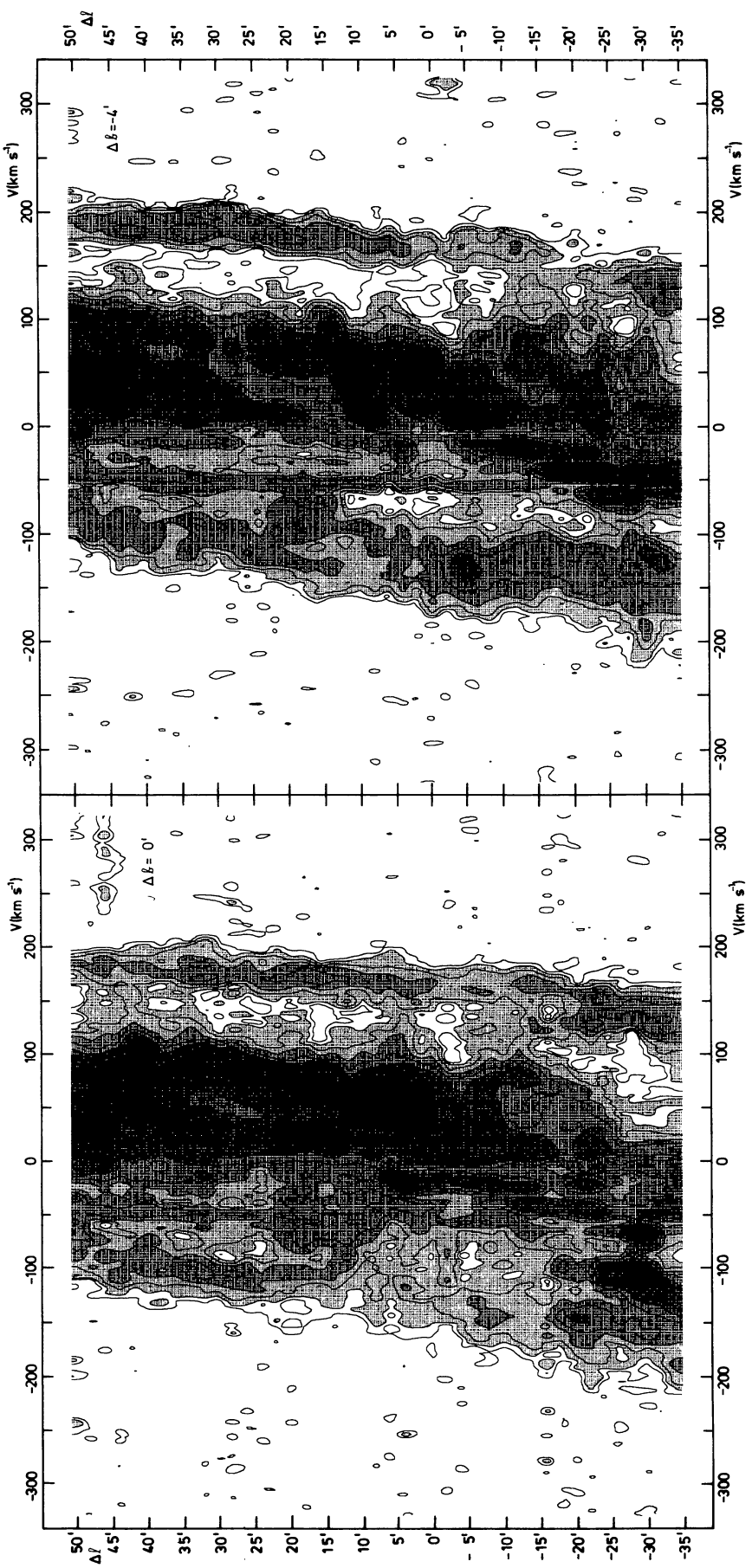

FIGURE 2c.

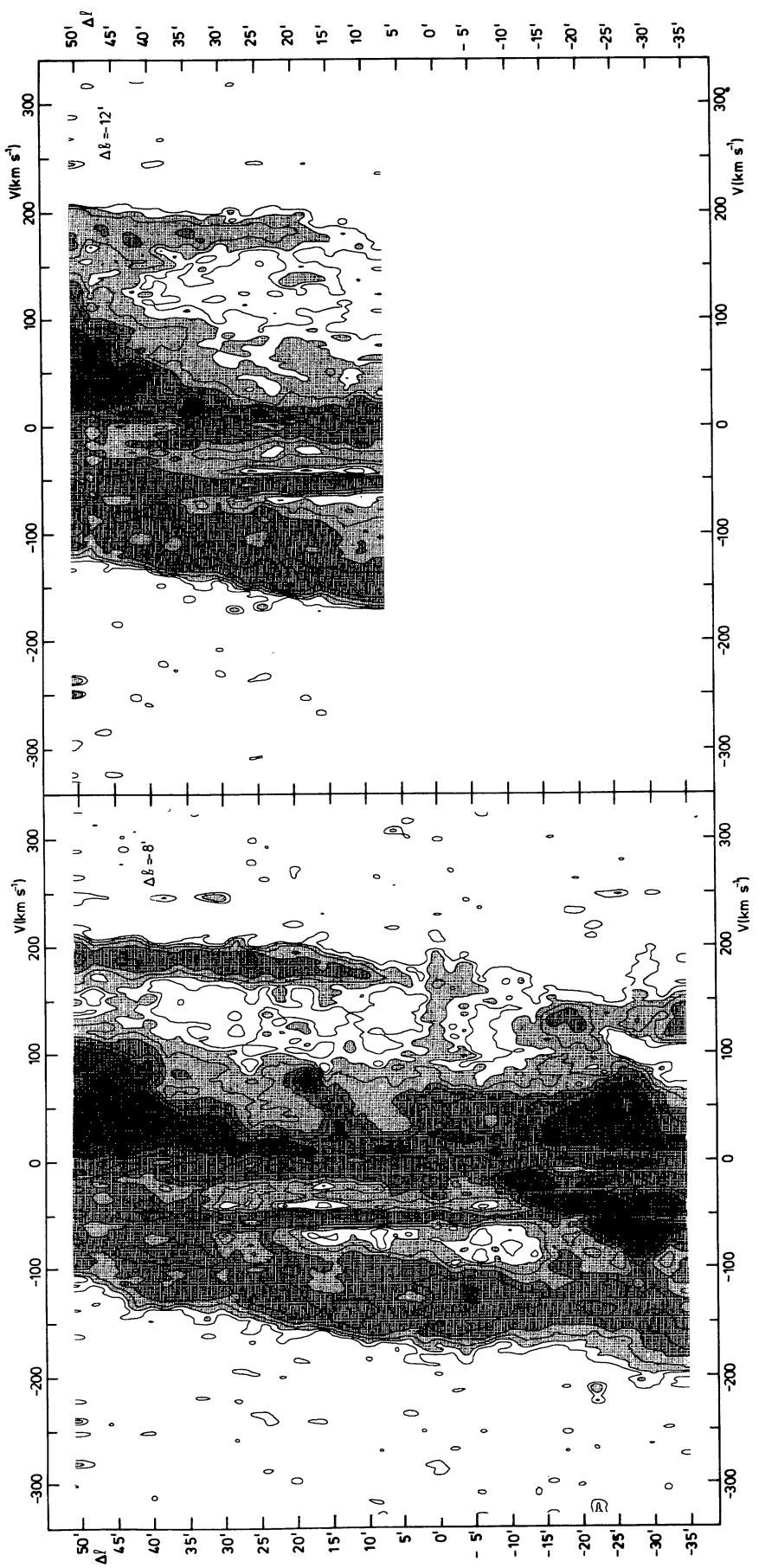

FIGURE 2d.

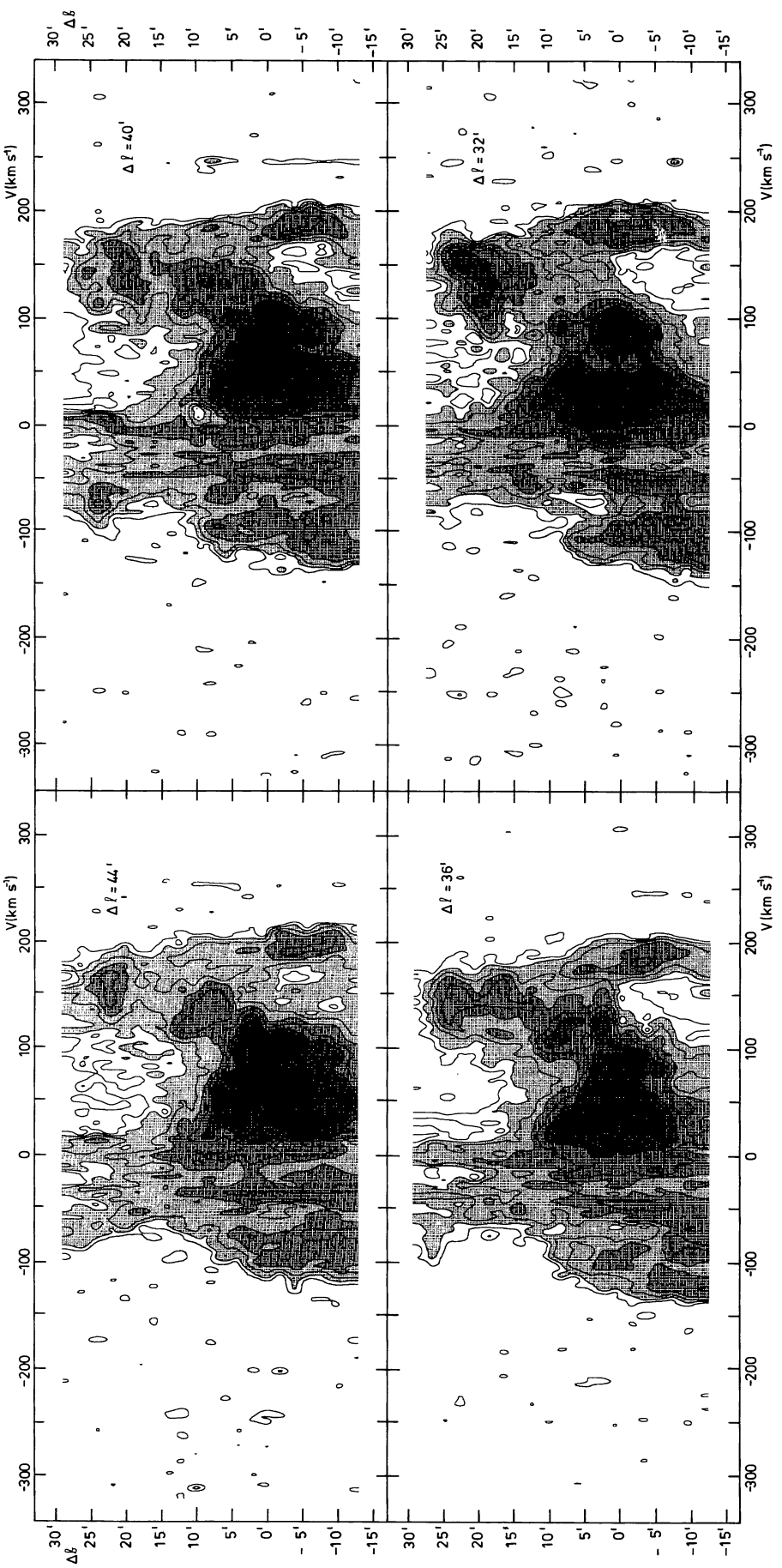

FIGURE 3. Latitude, velocity diagrams at 4′ intervals of galactic longitude; the latitude spacing of the data is 2′. Contour levels are drawn as in Figure 2.

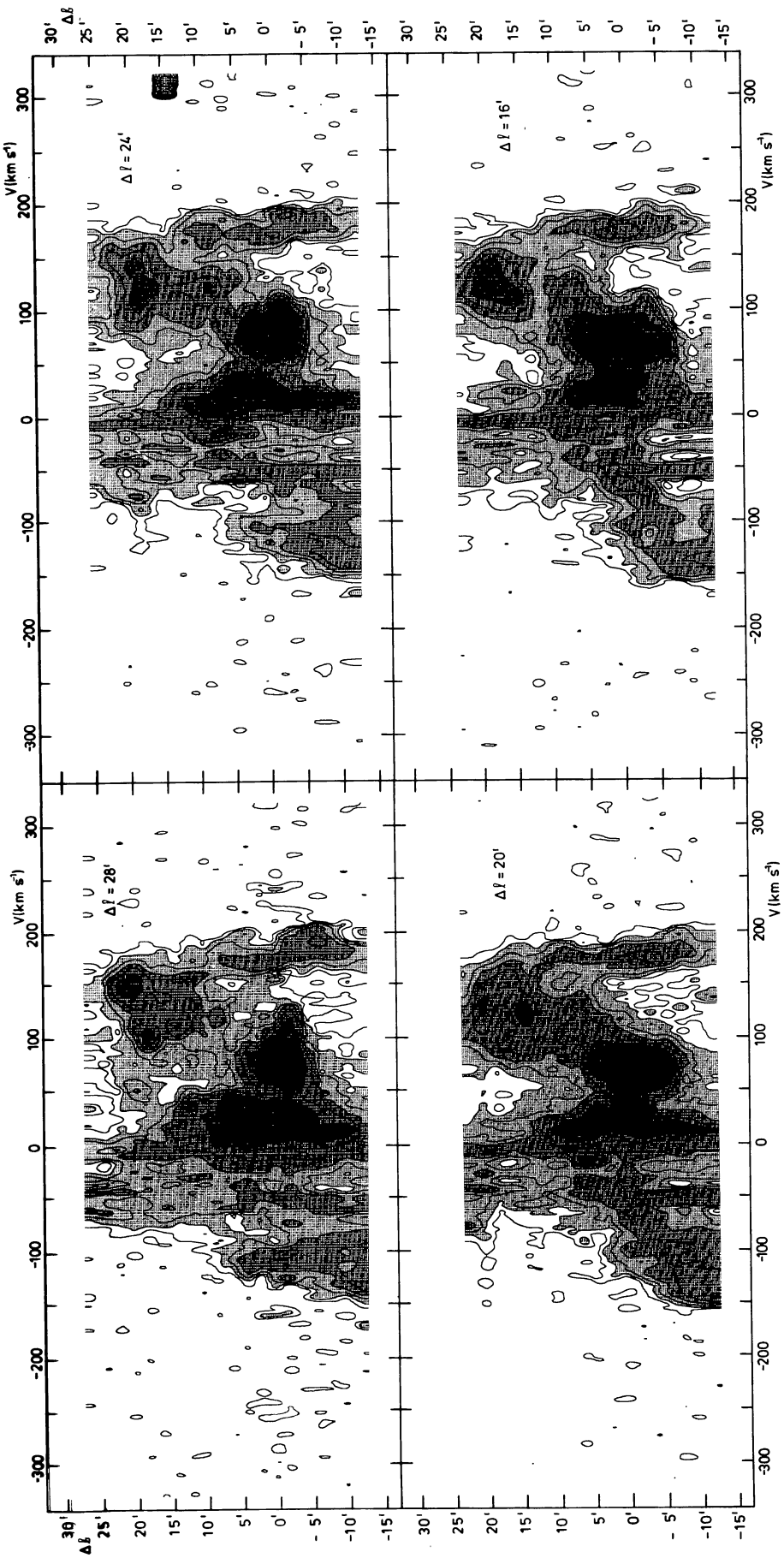

FIGURE 3. (*continued*)

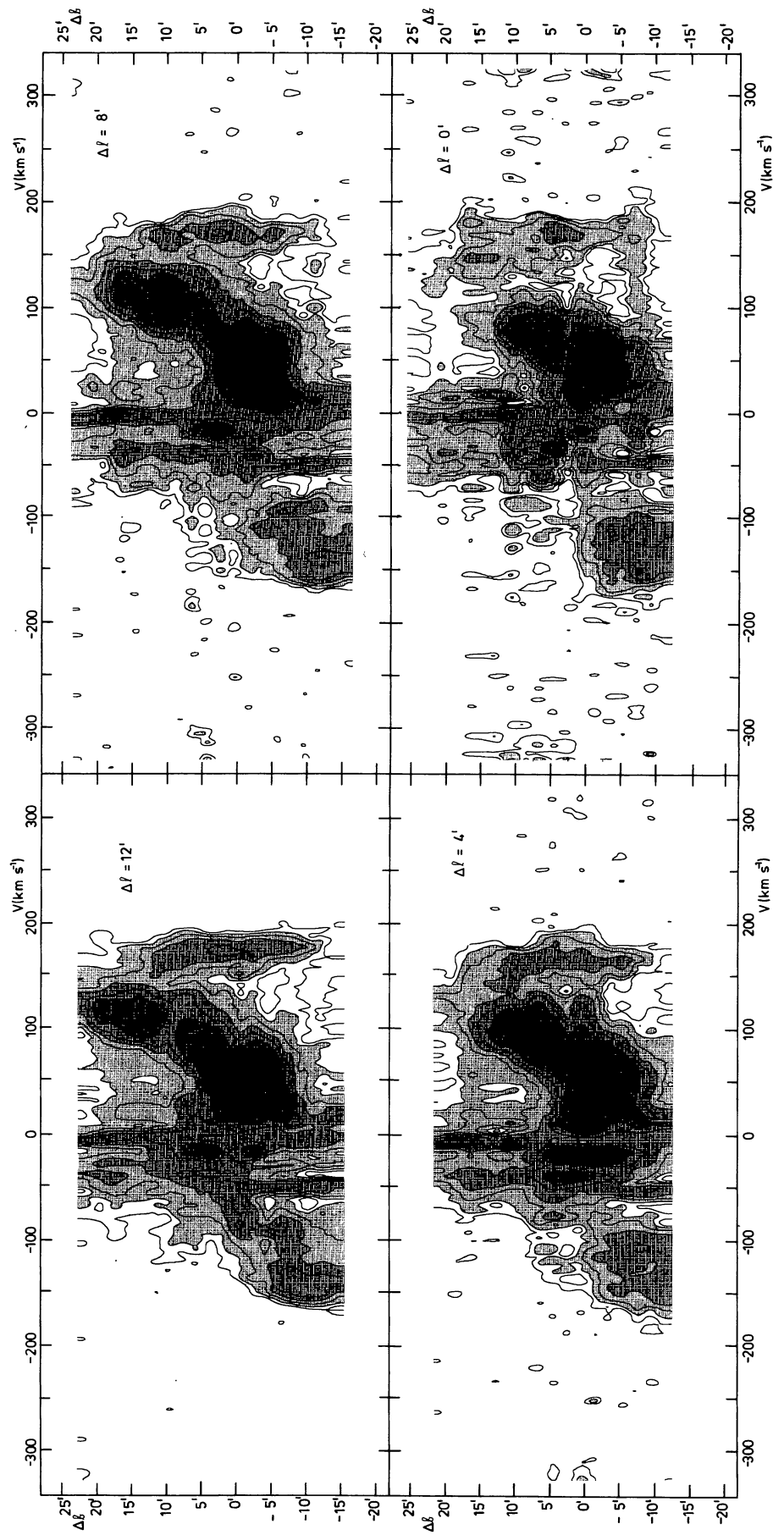

FIGURE 3. (*continued*)

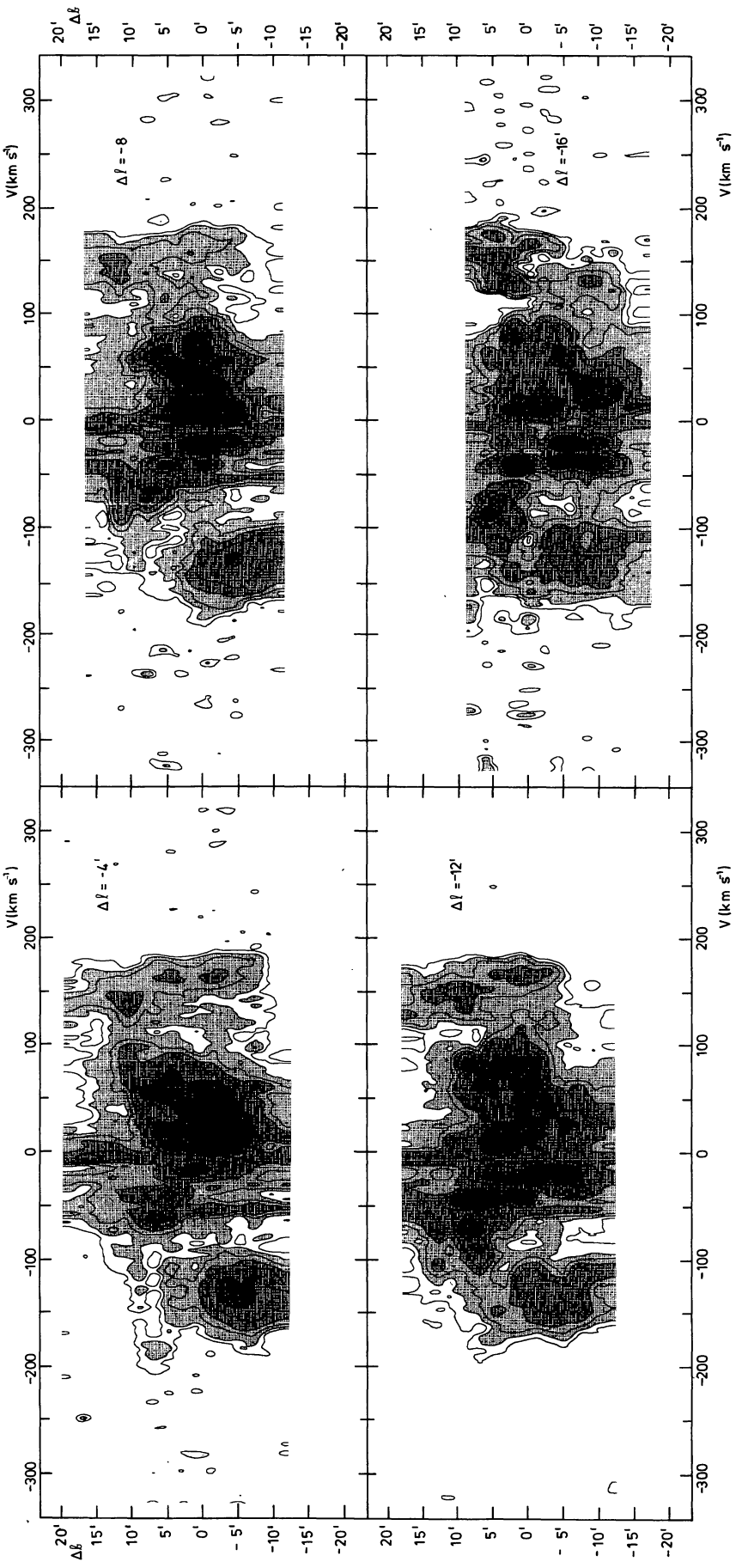

FIGURE 3. (*continued*)

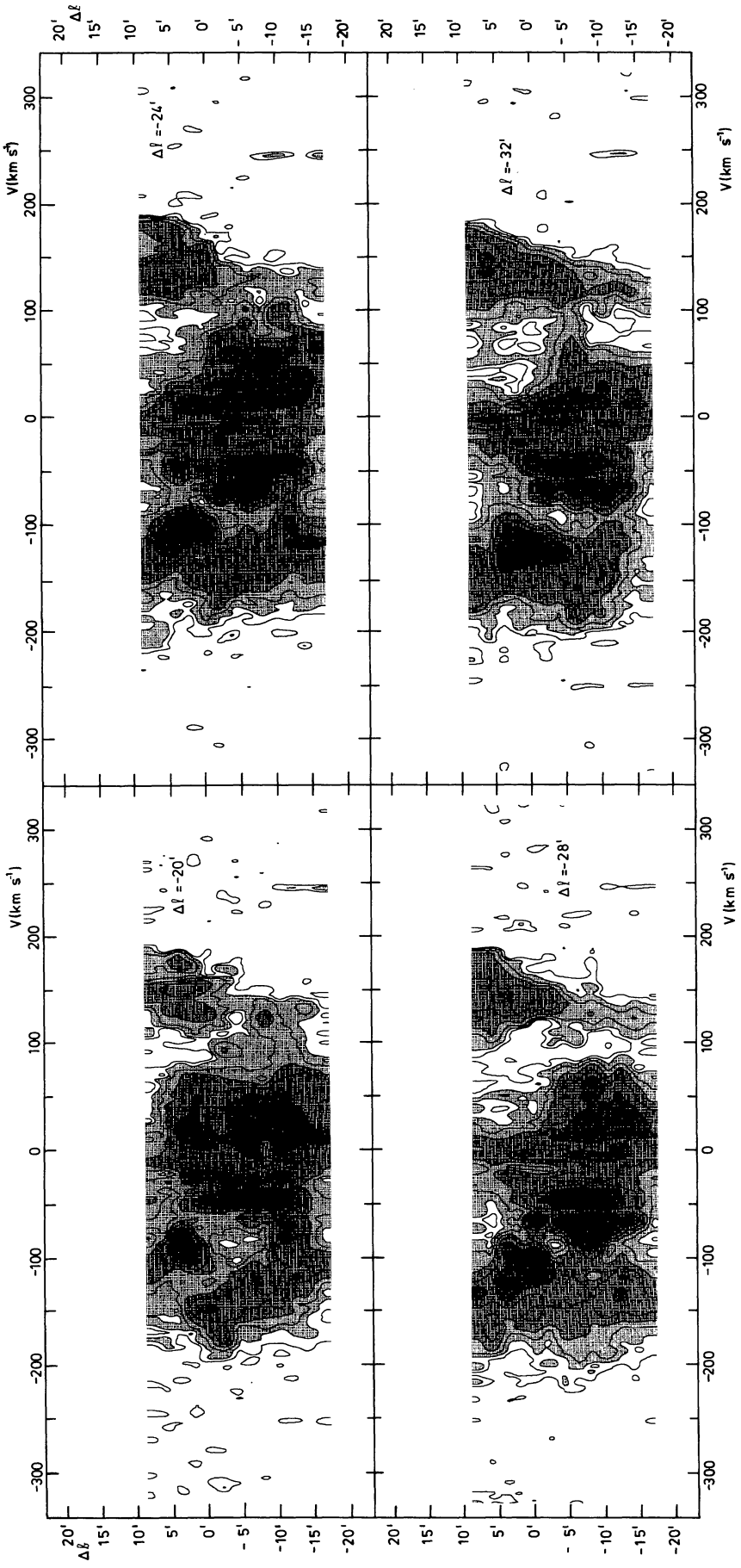

FIGURE 3. (*continued*)

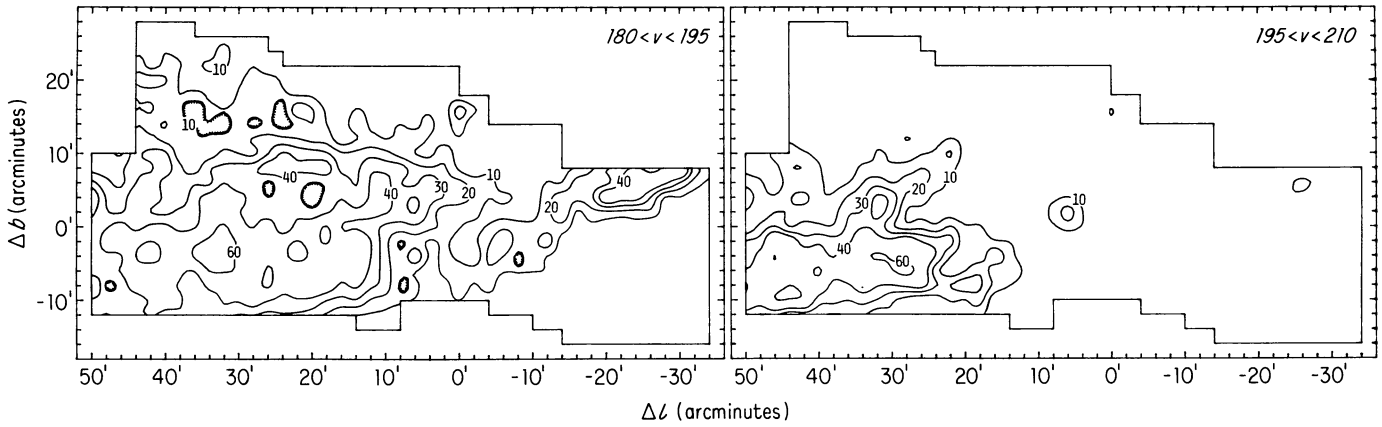

FIGURE 4a.

FIGURE 4. Integrated intensity maps taken over 15 km/s intervals spaced 15 km/s. Contours are labelled in units of K km/s.

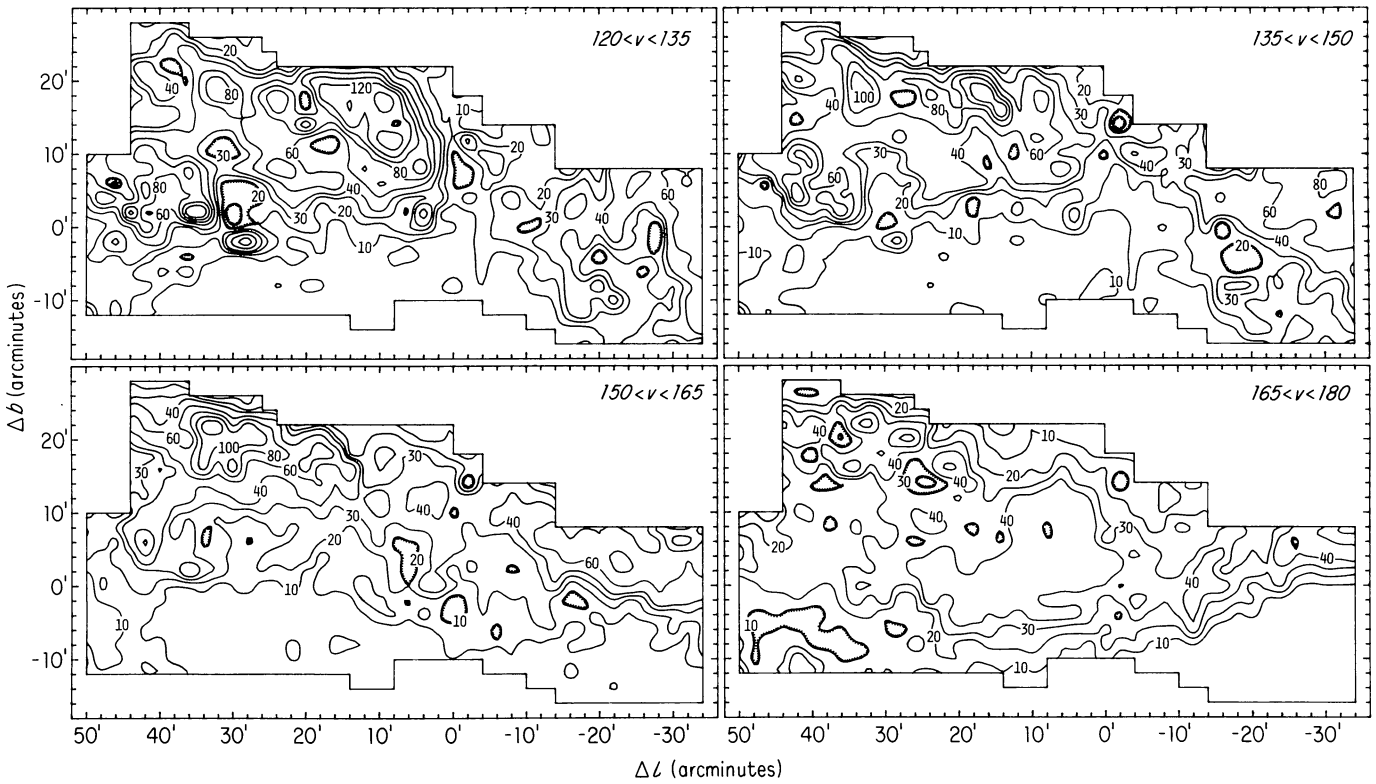

FIGURE 4b.

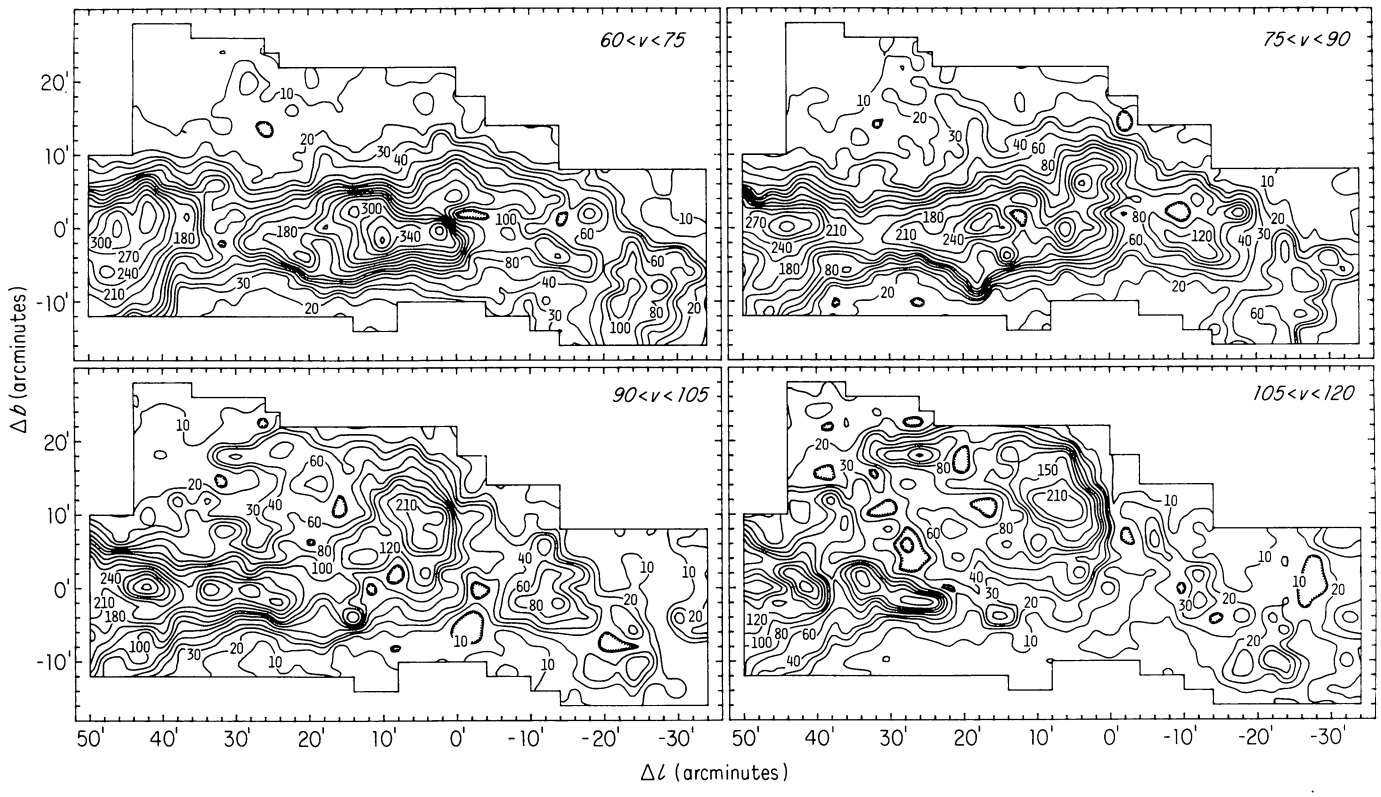

FIGURE 4c.

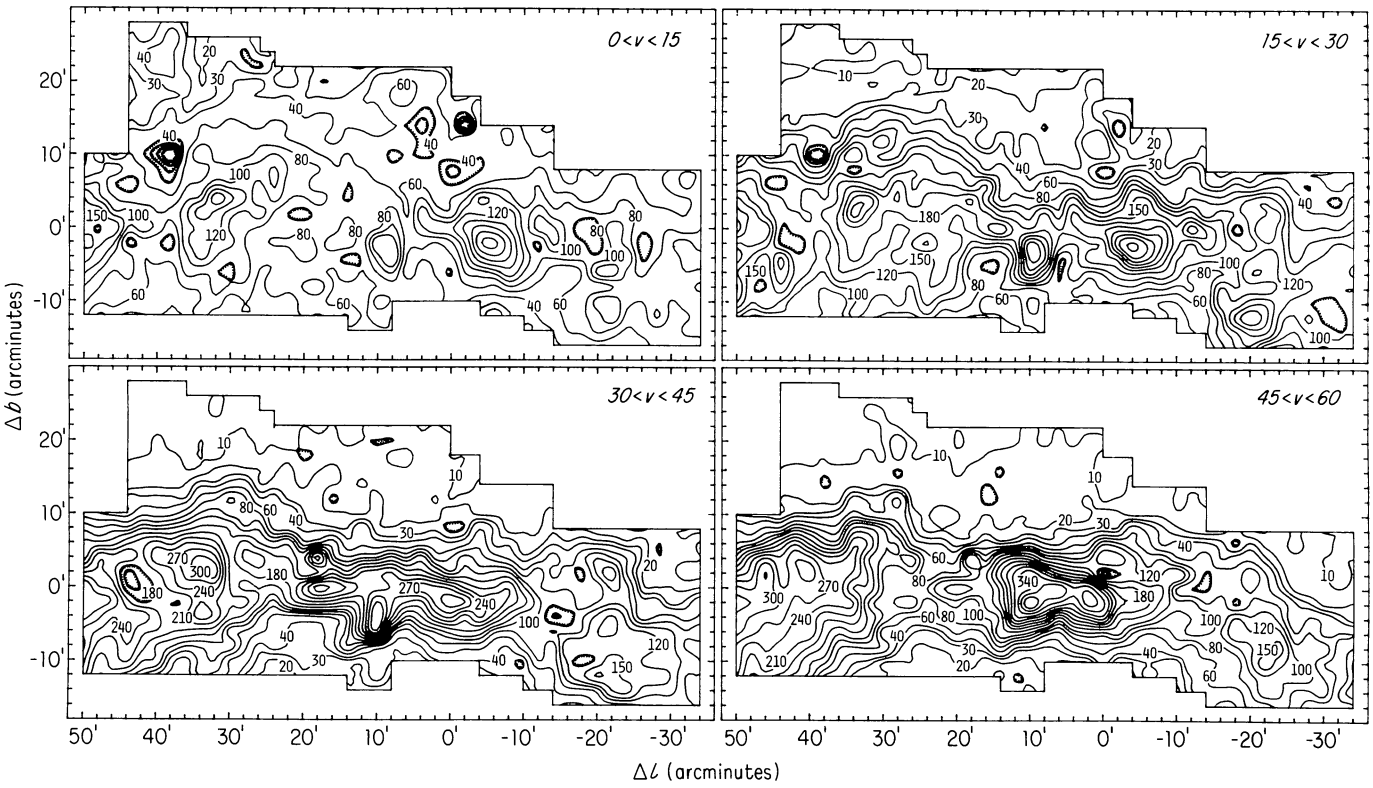

FIGURE 4d.

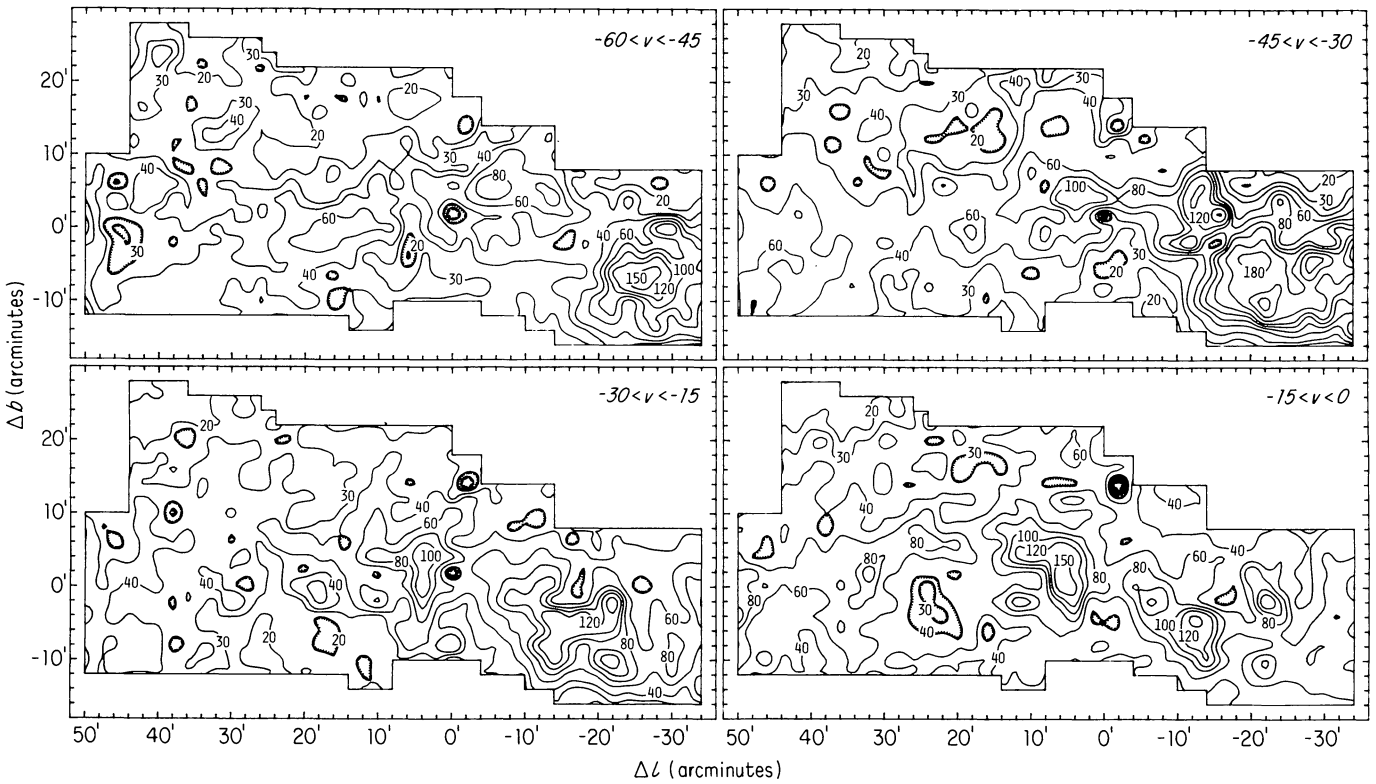

FIGURE 4e.

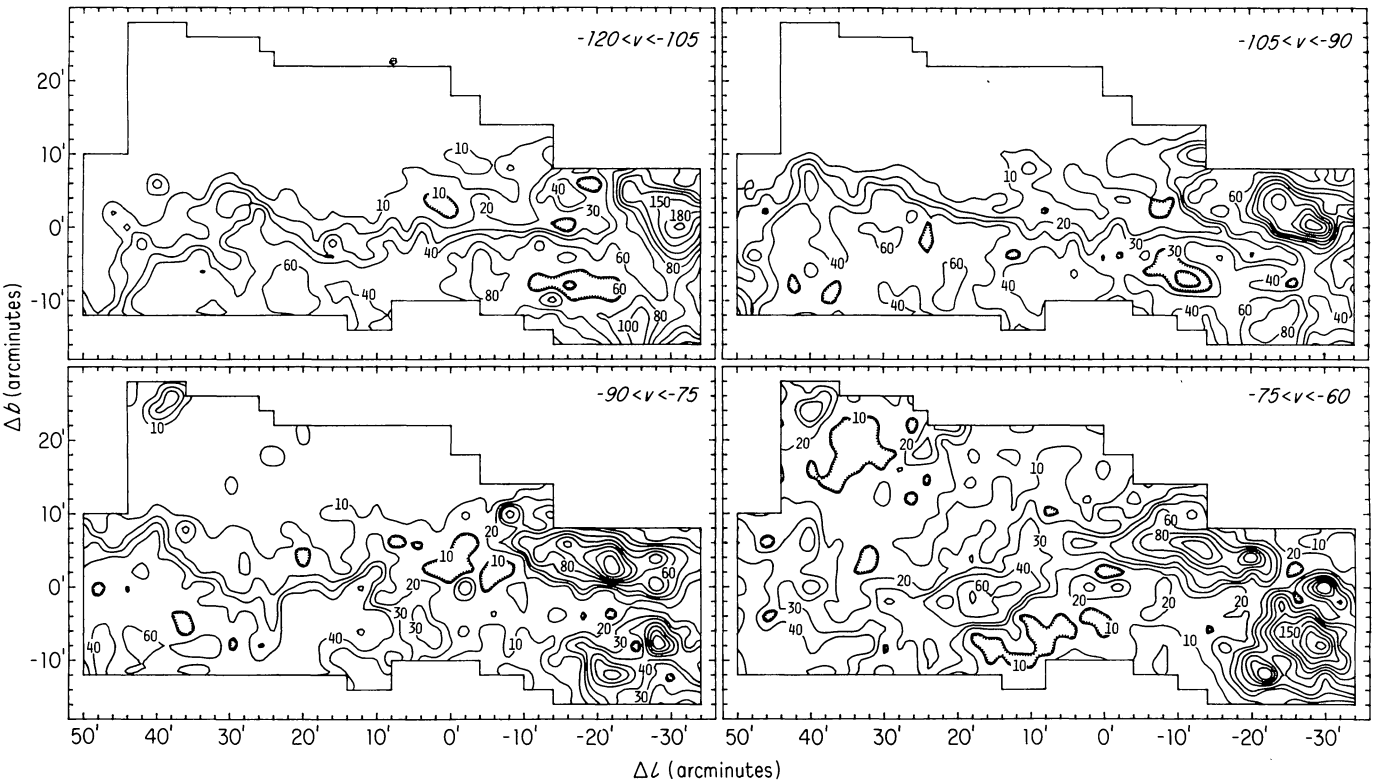

FIGURE 4f.

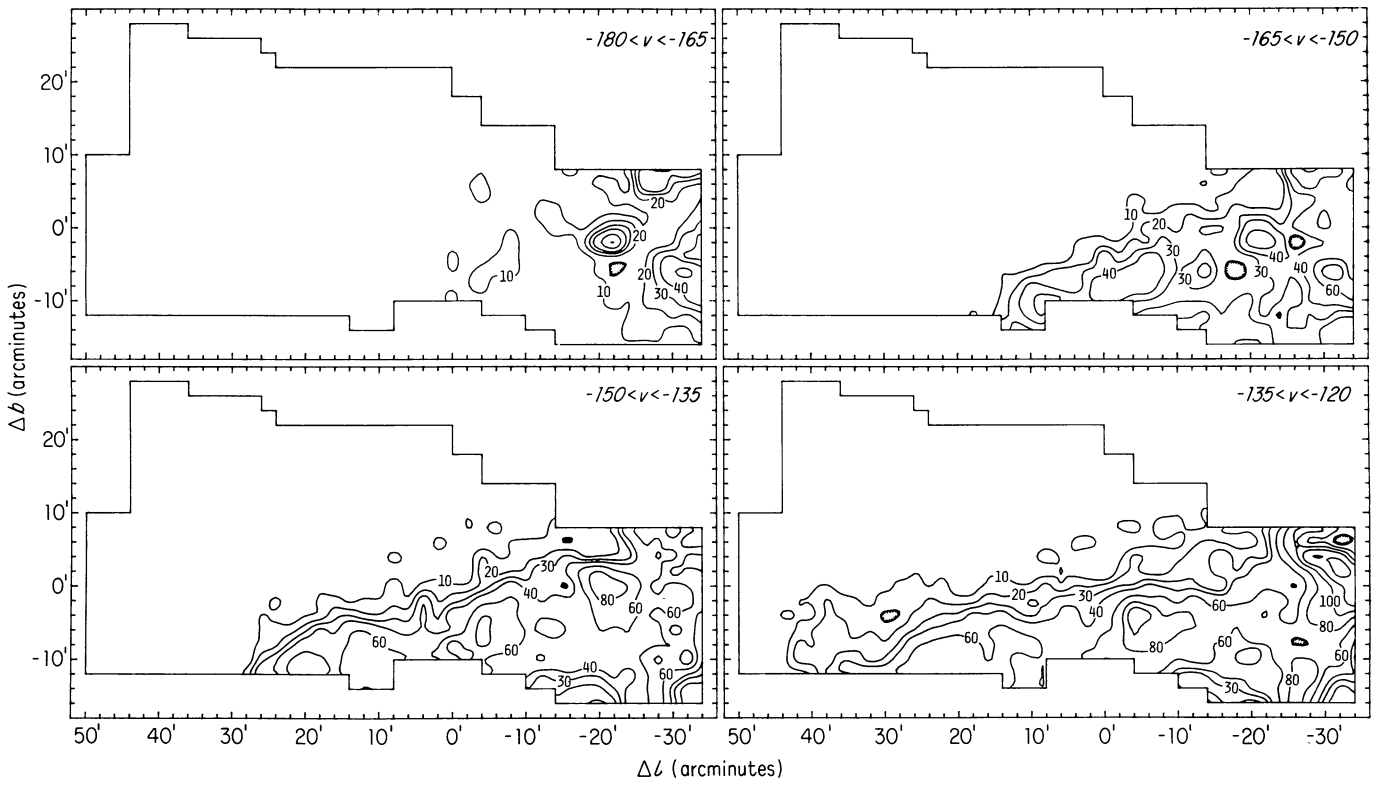

FIGURE 4g.

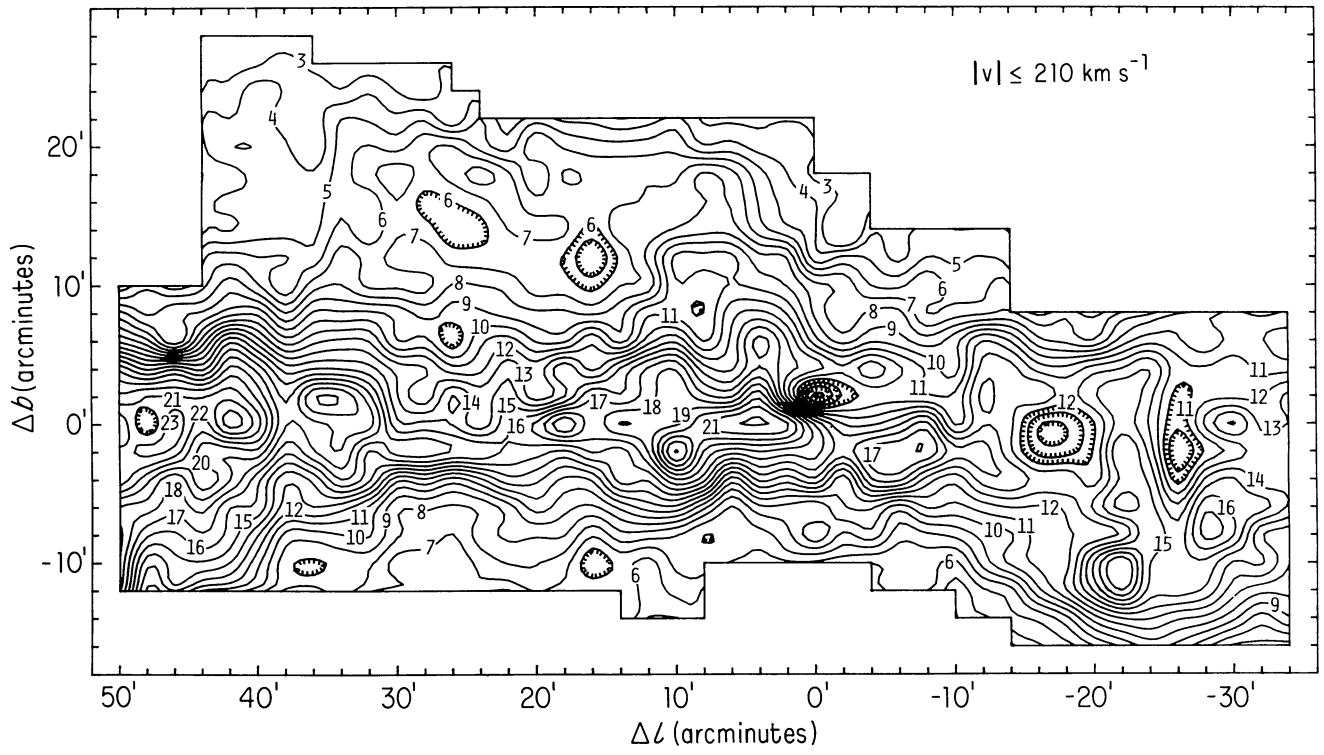

FIGURE 4h. Intensities integrated over the entire velocity range $| v | \leq 210$ km/s. Contours are labelled in units of 100 K km/s.

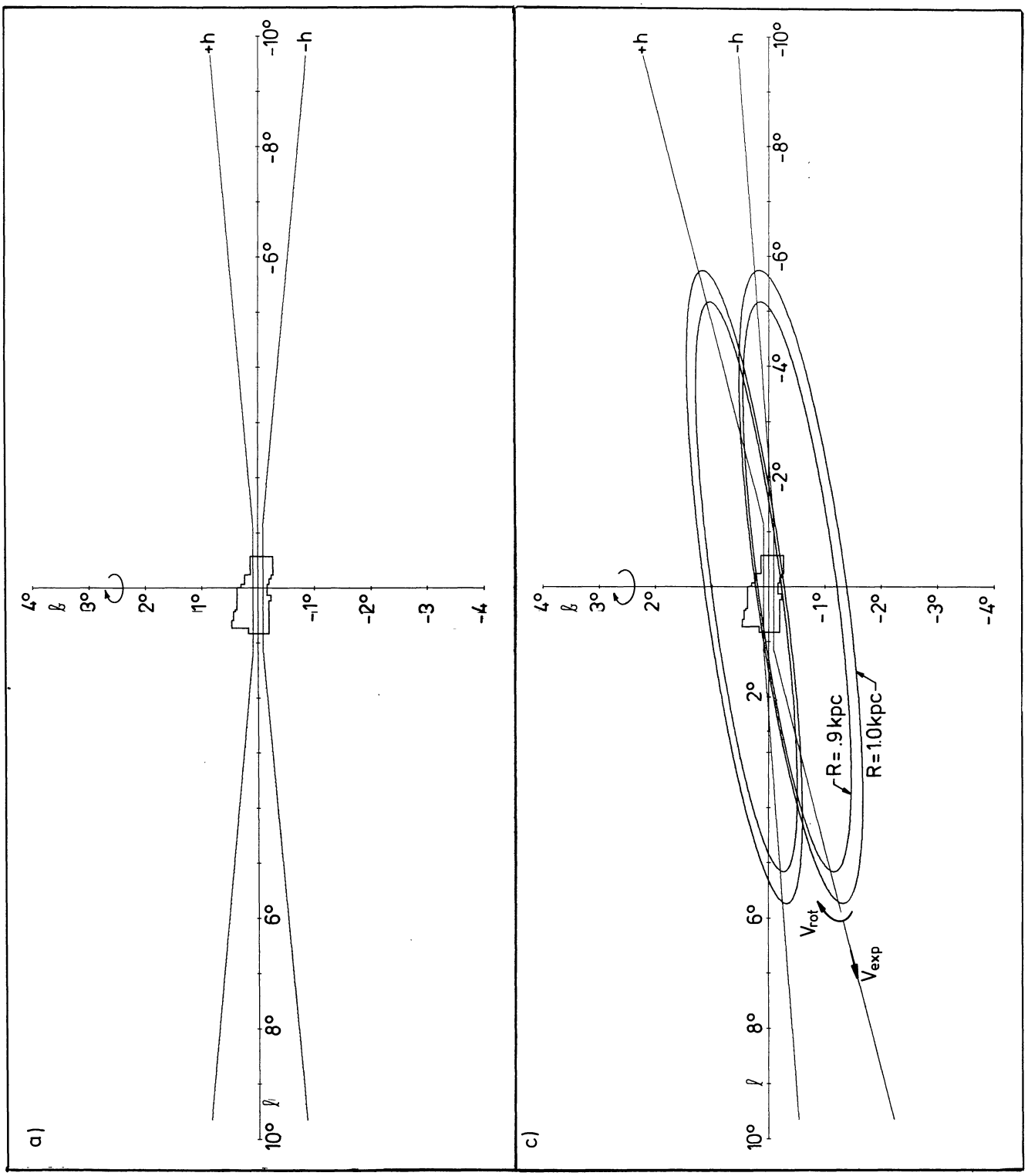

FIGURE 5.

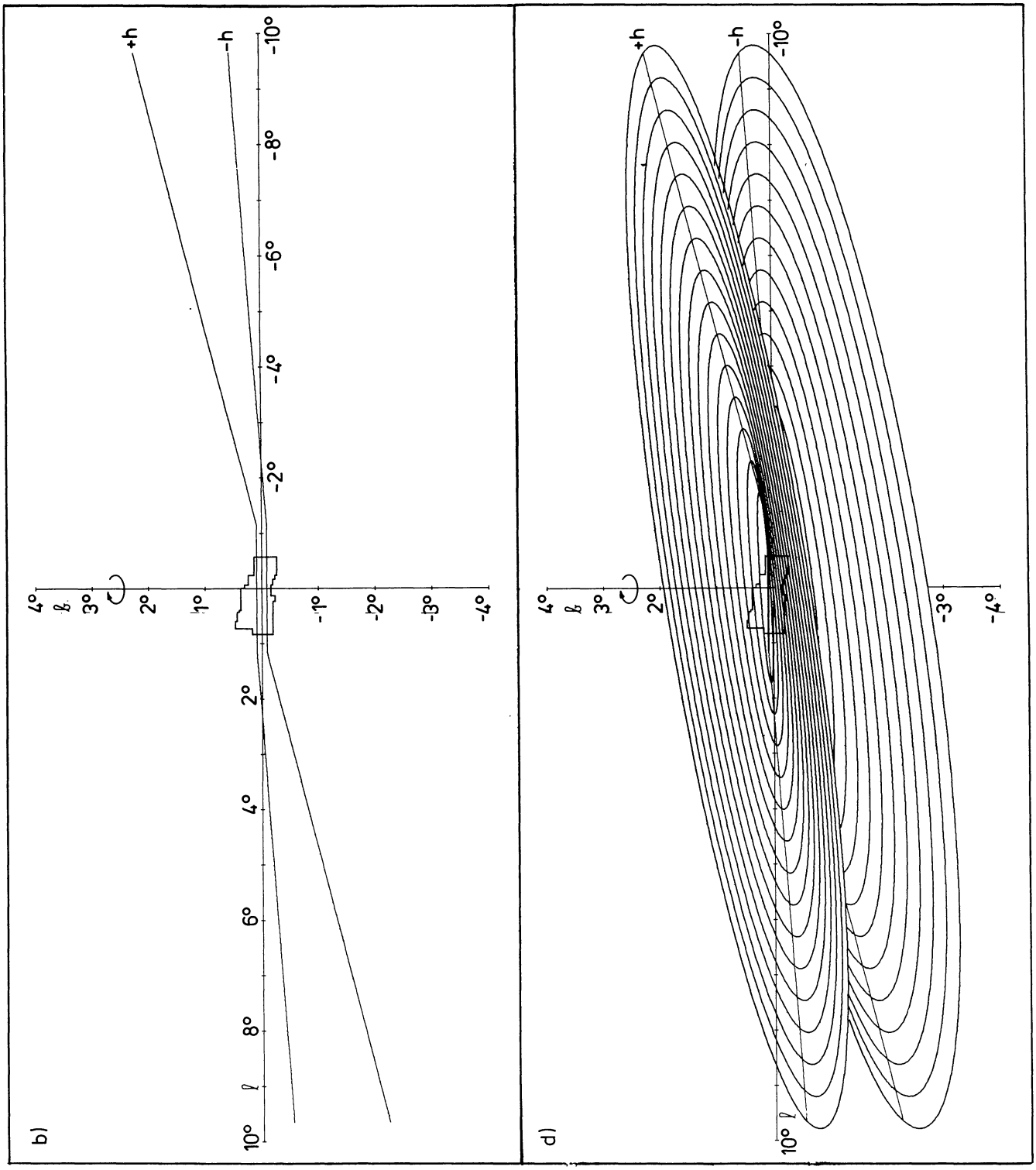

FIGURE 5.

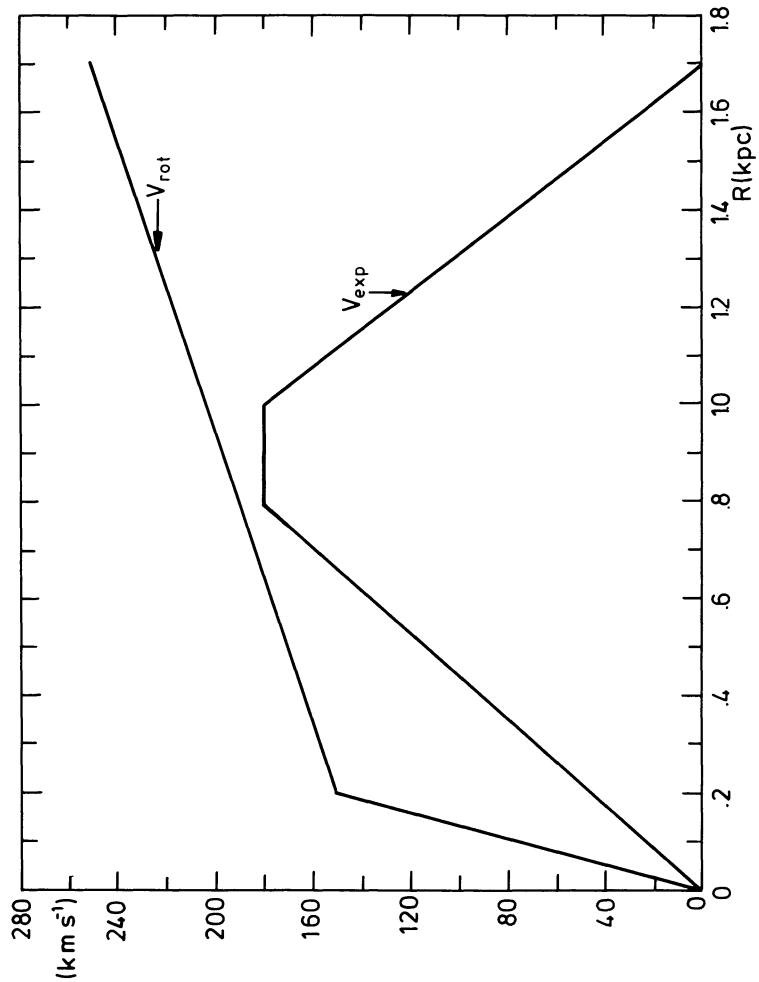

FIGURE 6.

Expansion and rotation components used in the modelling of the warped, tilted disk.

FIGURE 5. Representation of the geometry of the warped, flaring gas distribution of the model described in the text. The drawings show, to scale, projections onto the plane of the sky in the observationally relevant angular coordinates. The outline of the grid of CO observations is shown in each panel. a) Cross section showing the extent of the modelled disk and its flaring, with no warp. The lines represent one scale height above, and one below, the midplane of the disk, along galactocentric azimuths 90° and 270°. b) Same cross section as in panel a), but with the disk warped. The maximum warp angle, 13°, varies sinusoidally with azimuth. The line of nodes of the warp lies along azimuths 135° and 315°. c) Same cross section as in panel b), but with projection indicated of rings at $R = 900$ and 1000 pc, at one scale height above and below the mean disk. Although the observed grid does not extend far from the galactic center, if the galactic-core gas distribution does have the geometry modelled then gas at substantial distances from the center is sampled by lines of sight within the observed grid. d) Projections in the warped, flaring disk as in panel c), but with rings drawn at 100 pc intervals from $R = 0.1$ to 1.7 kpc, at one-sigma heights above, and below, the warped midplane. Portions of the lower-ring surface hidden behind the upper surface are not drawn. Although the mean (taken over all azimuths) of the midplane of the modelled disk coincides with the galactic equator, the projection appears inclined and resembles the tilted disk of our earlier Paper I model.

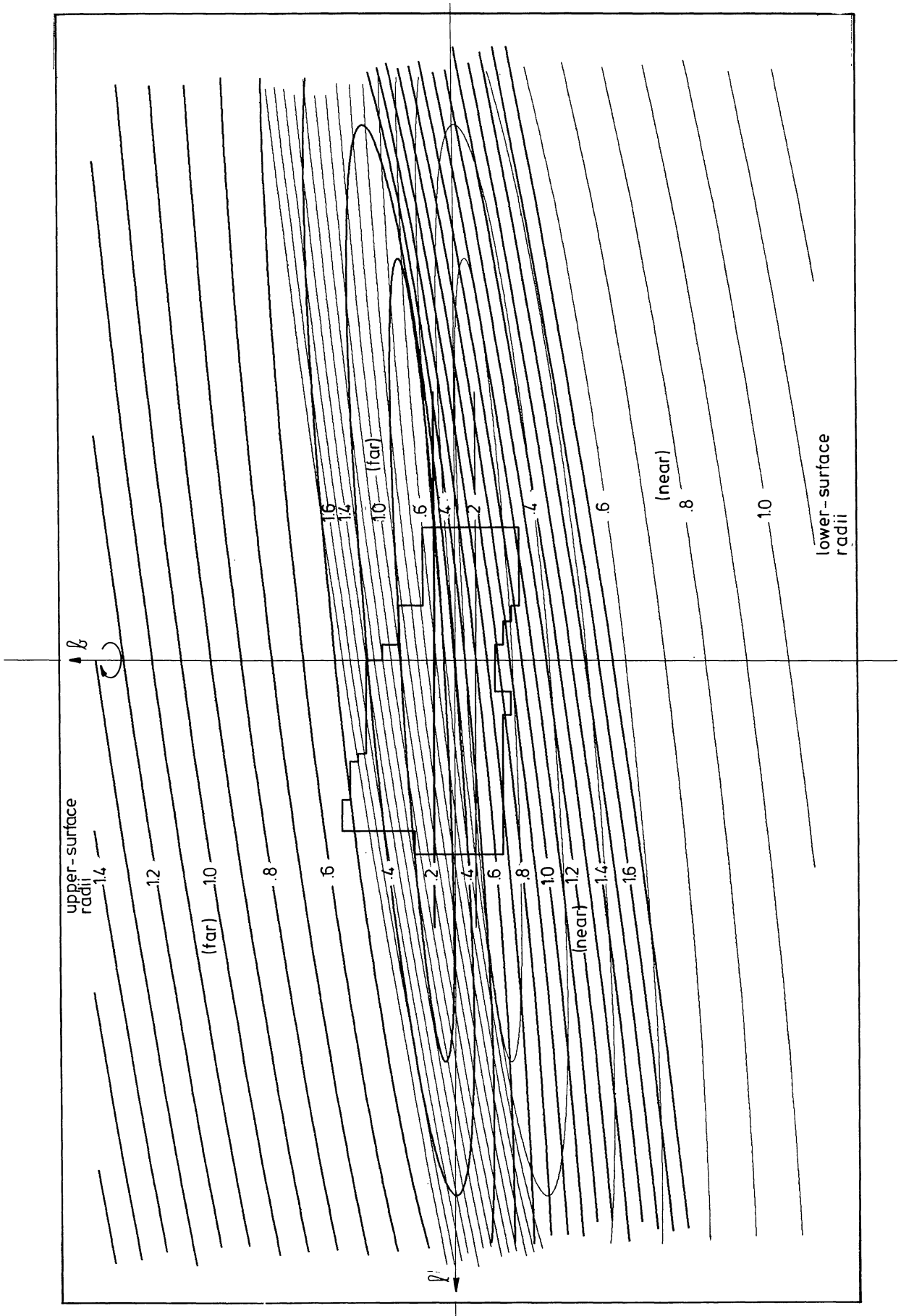

FIGURE 7. Enlargement of the observed-grid region of Figure 5d, showing projections of rings at 100 pc intervals over the range $0 < R < 1.7$ kpc. The "hidden" lines are not removed. According to this geometry, lines of sight on the observed grid points intercept long lengths of path; the crowding of the lines within the grid indicates that substantially different parts of the geometry will be sampled at closely adjacent grid points. It is in this context that we interpret the strong gradients in position and velocity which characterize the observations.

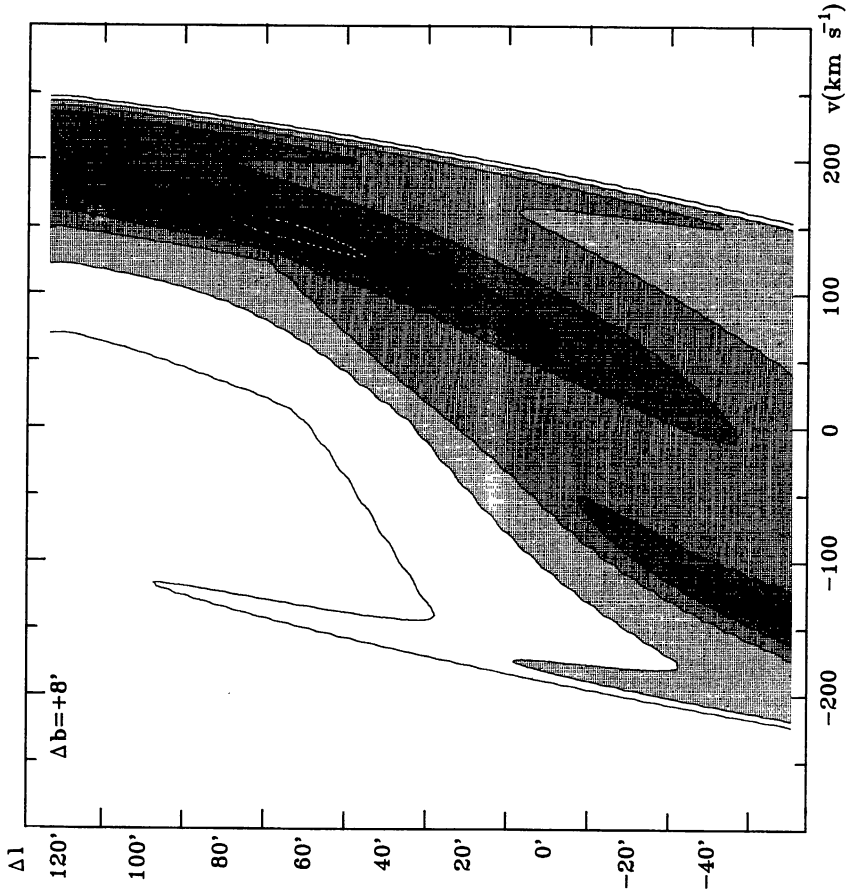

FIGURE 8b.

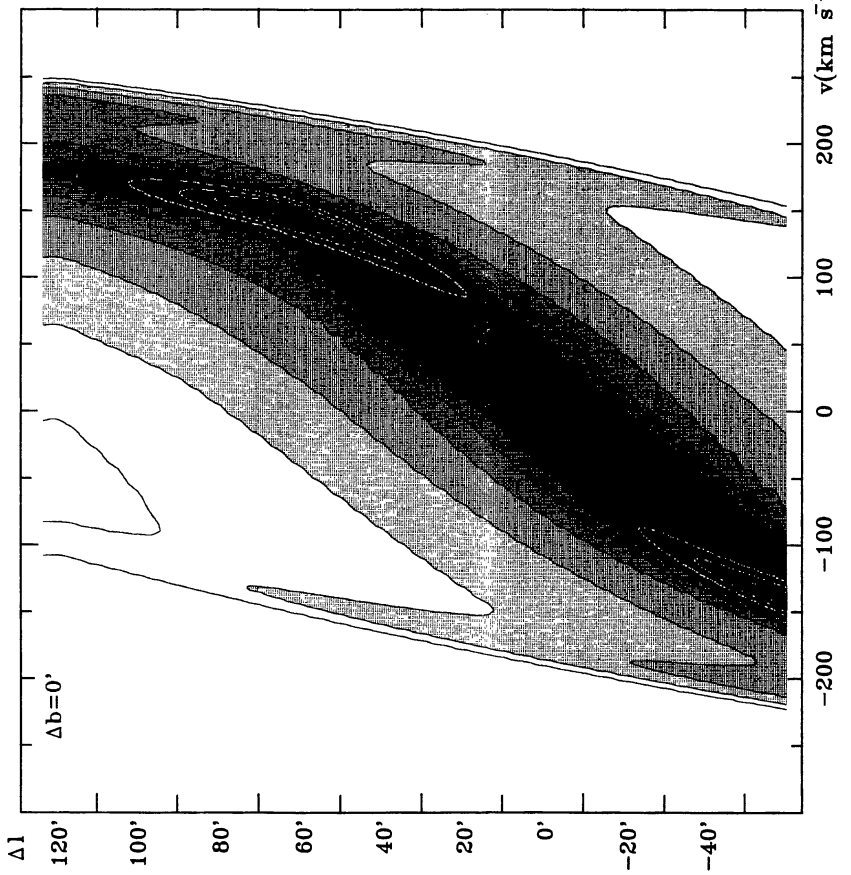

FIGURE 8a.

FIGURE 8. Synthetic longitude-velocity maps at the indicated latitudes from the warped, flaring disk model described in the text. These maps may be compared with the observed l, v situation shown in Figure 2. The contour levels are drawn as in Figure 2. a) Synthetic l, v map at $\Delta b = 0'$. The principal emission patterns produced by the model are the extreme-velocity bands which we associate with the "expanding molecular ring" feature, and the skewed, broad pattern at less extreme velocities, crossing $v = 0$ km/s near $\Delta l = 0'$, which is contributed by material in the thin, flat disk at $R < 200$ pc. b) Synthetic l, v map at $\Delta b = +8'$. Comparison of this map with the comparable observed situation shown in Figure 3 shows that they have the following principal trends in common: the intermediate-velocity, rotation-signature, component is predominant at positive l and v; the negative l and v pattern does not join in a continuous fashion with the dominant pattern; the extreme-velocity band in the $l < 0'$, $v > 0$ km/s quadrant dominate that in the $l > 0'$, $v < 0$ km/s quadrant. c) Synthetic l, v map at $\Delta b = +20'$. Comparison with the observed situation shown in Figure 3 shows the common broad emission pattern at positive velocities, with no negative velocity counterpart, and kinematics predominantly by expansion. d) Synthetic l, v map at $\Delta b = -8'$. Comparison of this map with the observed situation shown in Figure 3 shows that the model and observations share the following trends: the intermediate-velocity, rotation-signature component is predominate at negative l and v; that component pattern does not join in a continuous manner across $l = 0'$ with a positive l and v counterpart; the extreme-velocity band in the $l < 0'$, $v < 0$ km/s quadrant dominates the one in the $l < 0'$, $v > 0$ km/s quadrant.

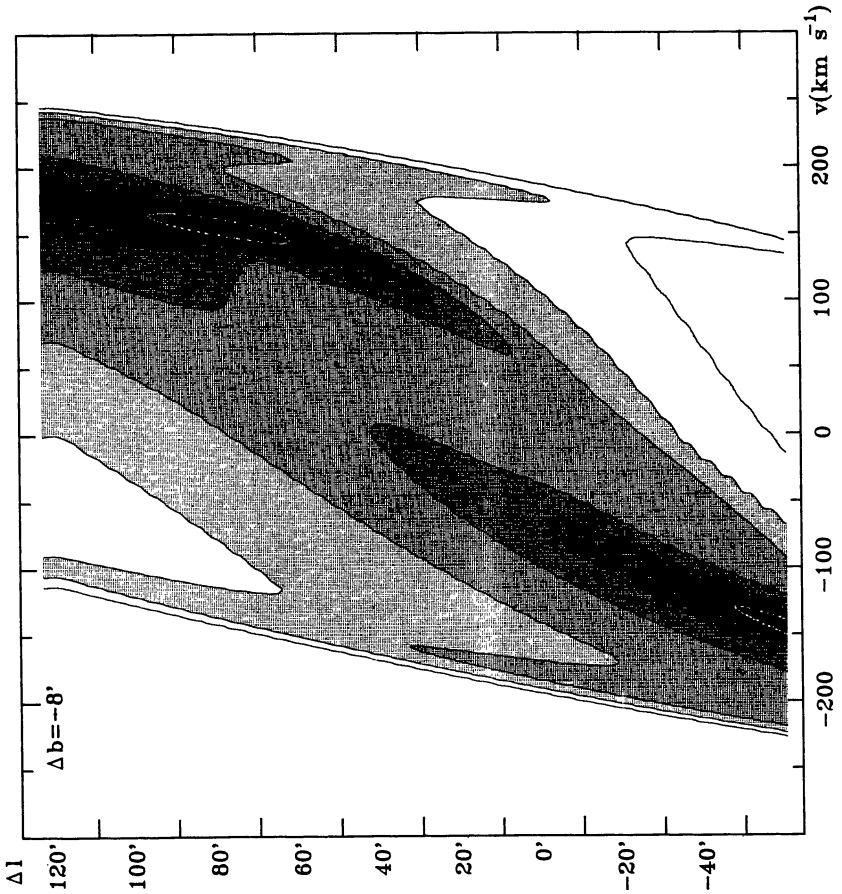

FIGURE 8d.

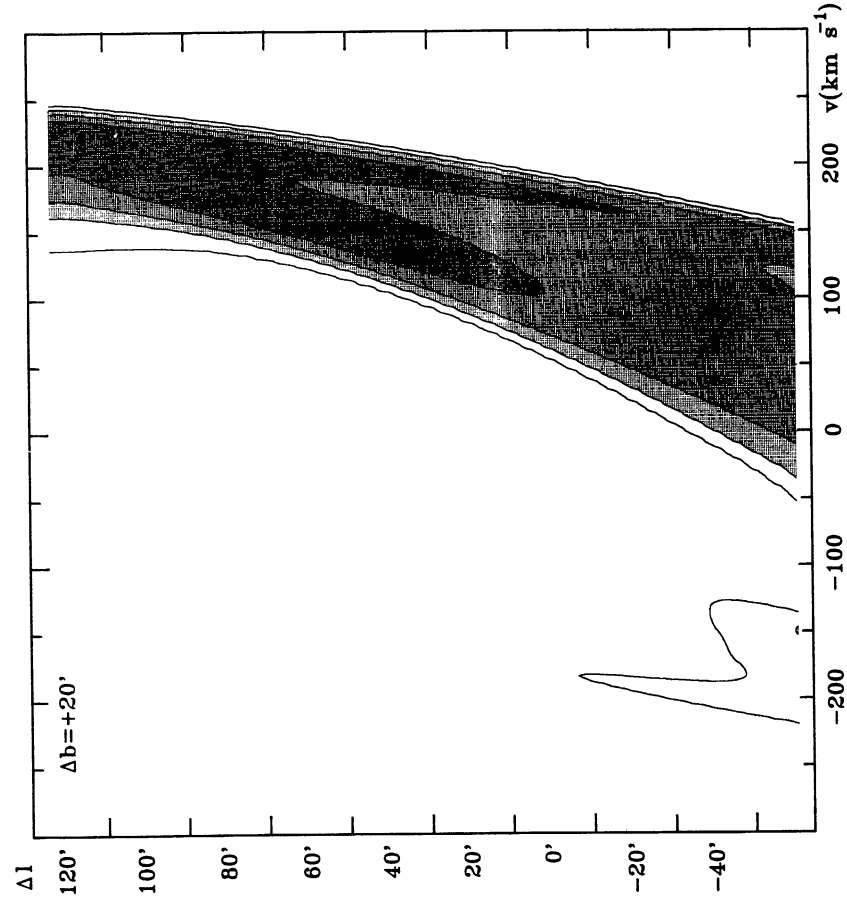

FIGURE 8c.

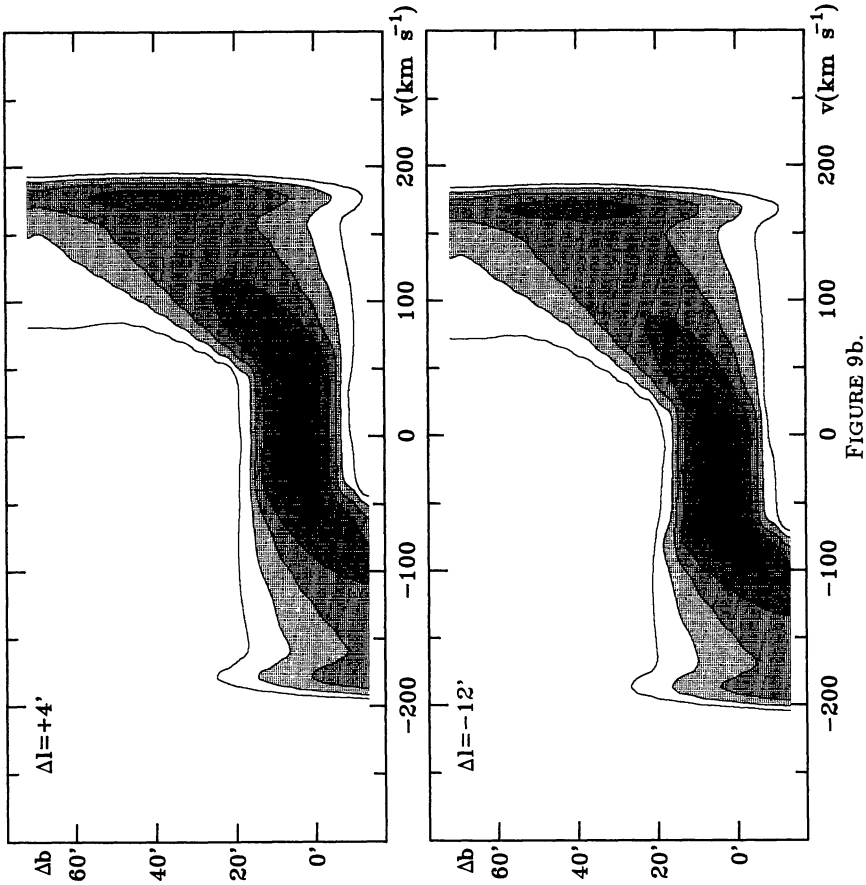

FIGURE 9a.

FIGURE 9b.

FIGURE 9. Synthetic latitude-velocity maps at the indicated longitudes of CO emission from the warped, flaring disk model. These maps may be compared with the observed b, v situation shown in the lower-left panels of Figure 3. The contour levels are drawn as in Figure 3. Comparison reveals the following common trends: 1) the intermediate-velocity pattern shifts in velocity with longitude exhibiting its rotation signature, but it remains centered near $b = 0'$; 2) the extreme-velocity bands exhibit a definite tilt in the sense that the pattern predominates in the quadrants $b > 0'$, $v > 0$ km/s and $b < 0'$, $v < 0$ km/s; 3) the flat-disk, intermediate-velocity pattern blends with the higher $|b|$, higher $|v|$ gas, and where it blends it shows an emission pattern with a strong $\Delta b/\Delta v$ gradient; this gradient becomes steeper with increasing Δl.